

**NASA Contractor Report 182020**

**INTEGRATED CONTROL/STRUCTURE DESIGN**

**J. A. Bossi,  
K. S. Hunziker,  
and  
R. H. Kraft**

**Boeing Defense and Space Group  
Aerospace & Electronics Division  
P.O. Box 3999  
Seattle, WA 98124-2499**

**Contract NAS1-18762  
December, 1990**

(NASA-CR-182020) INTEGRATED  
CONTROL-STRUCTURE DESIGN Final Report  
(Boeing Aerospace Co.) 65 p CSCL 01C

N91-15180

Unclas  
G3/08 0325587



National Aeronautics and  
Space Administration

**Langley Research Center**  
Hampton, Virginia 23665-5225

# Integrated Control/Structure Design

Joseph A. Bossi, K. Scott Hunziker, and Raymond H. Kraft  
*Boeing Aerospace & Electronics, Seattle, Washington*

## Abstract

A new approach for the design and control of flexible space structures is described. The approach integrates the structure and controller design processes thereby providing extra opportunities for avoiding some of the disastrous effects of control-structures interaction and for discovering new, unexpected avenues for future structural design. A linear control formulation based on Boyd's implementation of Youla parameterization is employed. Control design parameters are coupled with structural design variables to produce a set of integrated design variables whose values are selected through optimization-based methodology. A performance index reflecting spacecraft mission goals is formulated and optimized with respect to the integrated design variables. Initial studies have been concerned with achieving mission requirements with a lighter, more flexible space structure. Details of the formulation of the integrated design approach are presented and results are given from a study involving the integrated redesign of a flexible geostationary platform.

## Introduction

The "Integrated Control/Structure Design" study was performed as Task #3 of the NASA contract "Aircraft and Spacecraft Guidance and Control Technology", No. NAS1-18762. The objective of this effort was the implementation and demonstration of a pilot computer code for the integrated design of actively controlled structures. Recognized from the outset was the need for a software environment that would facilitate the multi-disciplinary analysis involved. The Integrated Analysis Capability (IAC) software [1] was chosen to provide this framework. The IAC utilities provide not only an efficient data base system for engineering analysis but also easy access to analysis modules such as model generation, finite element analysis, control design, and simulation tools.

To accomplish the stated objectives, the following tasks were entailed (as written in the statement of work):

1. selection of a representative pilot integrated design problem and the appropriate analytical methods and computer software,
2. development and enhancement of the necessary IAC interfaces for the pilot integrated design problem,
3. demonstration of the pilot computer code for the selected design problem,
4. study of the issues involved in the formulation of practical performance functions and constraints, and
5. documentation of the work performed and plans for follow-on efforts.

Several significant accomplishments were made in the course of this research. By developing a method for calculating the open-loop modal response sensitivities without differentiating the structure's eigenvectors, we were able to avoid the difficult and involved method that is normally employed. By using a control formulation (based on the Youla parameterization) in which the controller responses themselves are parameters, we implemented a promising new approach and verified its usefulness for the kind of problems considered here. By implementing a software tool that can not only perform the integrated analysis of an actively controlled structure but also optimize its design for a wide range of possible objectives and constraints, we demonstrated that such optimization is practicable and that significantly better designs can result.

Besides meeting the original objectives, we have learned much about the problem and have identified several areas that may warrant further investigation. This document is the final report of the task and describes our objectives, methods, and findings.

## Analytical Approach and Implementation

The usual approach for designing large, flexible, space structures with active vibration suppression is a two-step procedure. The first step is to determine the structural design based on structural costs and open-loop dynamic behavior. Then, given this structural design, the second step is to design the control system to obtain the desired closed-loop dynamic behavior. These two steps may be iterated until a suitable design is obtained.

This sequential approach is fairly straightforward; however, it makes it difficult (and entirely reliant on the designer's experience and intuition) to exploit any coupling that may naturally exist between the two design problems. Because the structural design variables and the control design variables are considered separately, information regarding this coupling is not available to the designer. Consequently, there is no reason to expect this approach to converge even to a locally optimal design for most constrained problems.

The poor performance of the sequential approach is easily demonstrated. The simple optimization problem illustrated in Figure 1 has only two design variables and a single constraint; its feasible space lies above the constraint line shown. We might imagine that  $x$  is a structural design variable and that  $y$  is a control design variable. Consider the situation shown: the design currently under study lies on the constraint at the point A. Now if we are restricted to moving only along the  $x$  or  $y$  axes, as would be the case if the sequential approach were used, then the design cannot be improved without violating the constraint. A clear path to the minimum exists, but it can be taken only if the design variables can be modified simultaneously.

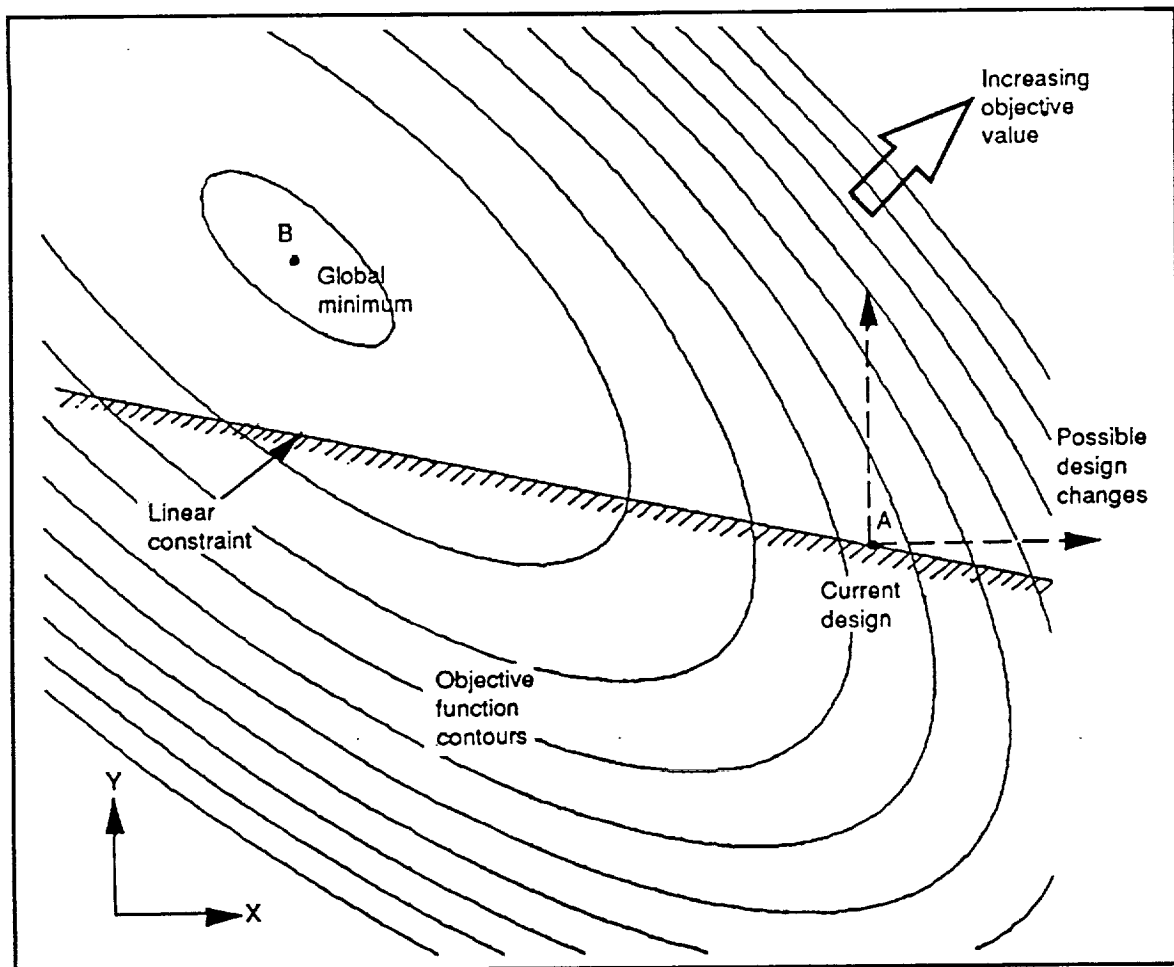


**Figure 1: A simple optimization example.**

For this reason, it seems likely that improved designs could often be found by considering simultaneously the complete set of design variables. This has been apparent to many, and a large number of studies are described in the literature. Some of this work has been directed toward formulating the combined problem in a manner similar to those of modern optimal control, several examples of which are described in References [2-5]. Unfortunately, these approaches tend to be quite restrictive in terms of the kinds of problems to which they apply. These restrictions typically preclude problems of practical complexity.

An alternative approach to simultaneous optimization is to use the methods of numerical optimization. This approach has a distinct advantage in that it is much less restrictive on the kinds of design variables, objectives, and constraints that can be considered. References [6,7] describe several applications of this approach.

Attempts to use numerical optimization methods, however, have been hampered by several difficulties. Because the objective and constraints are typically defined in terms of the closed-loop response of the structure, a complete structural and control analysis (with sensitivities) is required for every trial design. The effort involved can be prohibitive. This is particularly relevant to this multidisciplinary problem, since integrated analytical tools are generally unavailable. This is exacerbated when numerical differentiation is used to obtain the necessary gradients. Moreover, the dimensions of the design space and the complexity of the objective surface may also frustrate these optimization attempts.

The approach taken here for the integrated design problem is shown graphically in Figure 2. This approach was implemented in a computer program called *COSTAR*. Using a nonlinear programming method, an optimization module performs a search of design space, attempting to minimize the specified objective function while satisfying various constraints on its design and performance. The design space is comprised of both structural and control variables, and the optimizer is free to modify them simultaneously. We have attempted to avoid the principle obstacles to this type of approach by using efficient, integrated analysis tools, analytical gradient calculations, and design variables that tend to reduce the complexity of the objective surface.

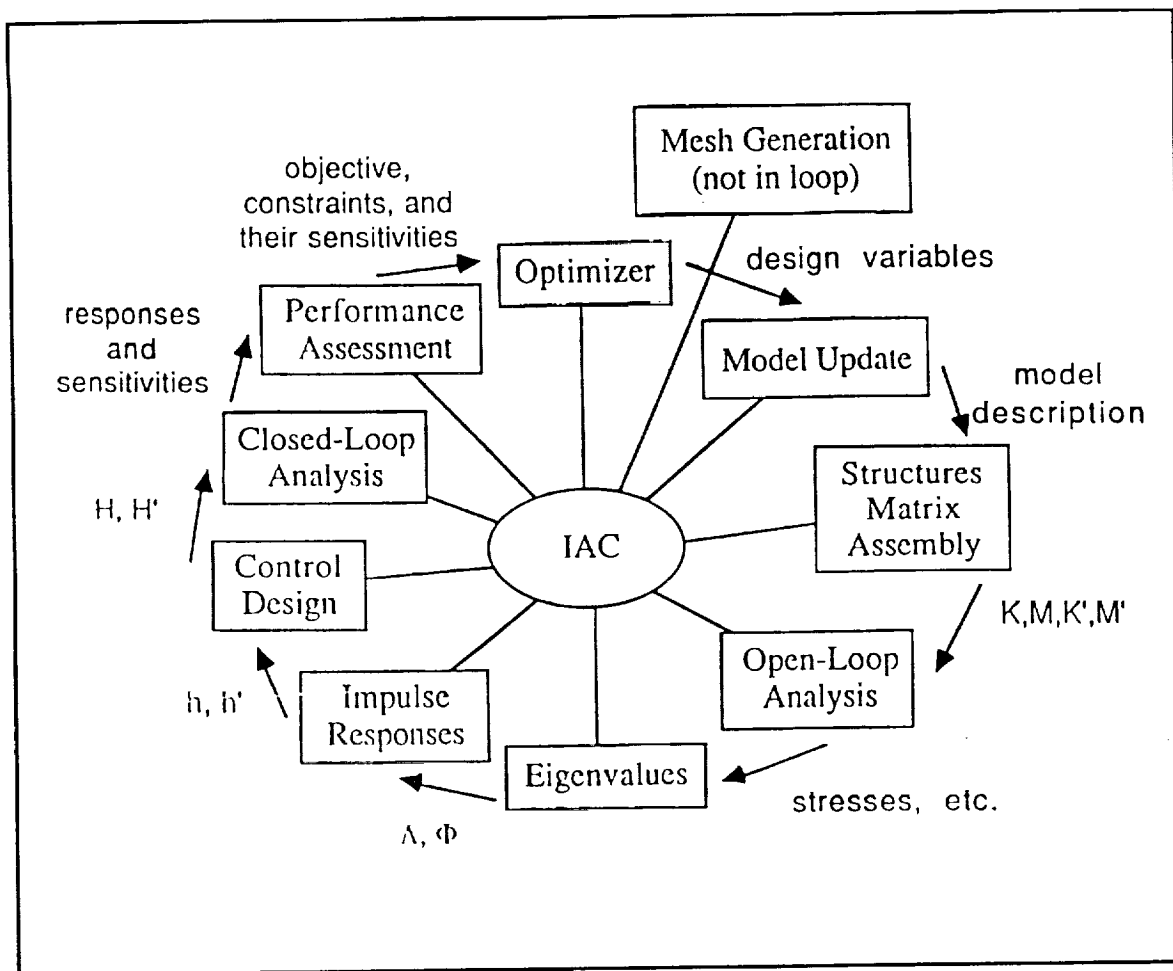


Figure 2: The COSTAR conceptual layout.

The functions that describe the objective and constraints are defined *a priori* by the user. Although this explicit description of the problem may require a significant effort from the user, the hallmark of this approach is that the type and form of the objective and constraint functions is restricted only in that they must be continuous functions of the design variables. In the demonstration problem, functions such as "peak error" and "peak torque" were included along with more conventional performance functions such as "total mass" and "mean-square error".

### Structural Modeling

In the COSTAR code, equations of motion for the structure are obtained by using the finite element method (FEM). A description of the structure is used by the FEM code to construct mass and stiffness matrices that characterize the structure. This description takes the form of several matrices that contain the connectivity, geometry, element properties, and material properties.

Table 1 lists the matrices that combine to describe the structure. As indicated, several of the matrices are functions of the design variables vector  $\mathbf{v}$ . Thus different choices for the design variable values result in different structures. Throughout this report, derivatives with respect to the design variables are indicated by a prime.

Matrix	Sensitivity	Description
$X$	$X'_i \equiv \frac{\partial X}{\partial v_i}$	Locations of the nodes
$P$	$P'_i \equiv \frac{\partial P}{\partial v_i}$	Element properties
$E$	$E'_i \equiv \frac{\partial E}{\partial v_i}$	Material properties
$A$	$A'_i \equiv \frac{\partial A}{\partial v_i}$	Element orientations
$\kappa$	$\frac{\partial \kappa}{\partial v_i} = 0$	Element connectivity
$\rho$	$\frac{\partial \rho}{\partial v_i} = 0$	Element property pointers
$\chi$	$\frac{\partial \chi}{\partial v_i} = 0$	Material property pointers
$\tau$	$\frac{\partial \tau}{\partial v_i} = 0$	Element types

**Table 1: Structural Definition Matrices.**

These matrices are themselves generated through the use of PATRAN [8] — a finite element pre-processor. The input to PATRAN (its “session file”) is kept in a parametric form so that changes to the values of the design variables can be easily accommodated. (The MACSYMA symbolic mathematics program [9] is used to update the PATRAN input file.) For reasons of efficiency, however, this kind of pre-processor cannot be used within the optimization procedure. The overhead involved in running this code would add significantly to the total execution time. Moreover, a finite difference procedure would be required to obtain sensitivities, adding greatly to the execution time and to the numerical errors in the sensitivities.

In many previous approaches to the simultaneous optimization problem, this problem has been avoided by representing the mass and stiffness matrices as explicit functions of the design variables. For example, it is common practice to prescribe them to be linear



functions of the design variables. Although this simplifies the analytical task, it imposes severe restrictions on the kinds of design variables that can be considered. In particular, it precludes the use of design variables that control the shape of the structure.

The COSTAR implementation avoids these difficulties by representing the structural model (that is, the description matrices listed in Table 1) as a linear combination of a set of *model variables*. The nodal locations, for example, are expressed as

$$X = \bar{X} + \frac{\partial X}{\partial \mu_1}(\mu_1 - \bar{\mu}_1) + \frac{\partial X}{\partial \mu_2}(\mu_2 - \bar{\mu}_2) + \dots \quad (1)$$

where  $\mu$  is the vector of model variables and the overbars refer to the baseline values. By specifying the model variables as possibly nonlinear functions of the design variables,

$$\mu_i = \mu_i(v) \quad (2)$$

relatively few restrictions are placed on the models. With this approach, the modeling software is used only to generate the model description. Updates for subsequent analyses (such as for optimization) proceed rapidly with only simple matrix operations involved. The sensitivities are obtained as

$$X'_i = \frac{\partial X}{\partial \mu_1}[\mu_1]'_i + \frac{\partial X}{\partial \mu_2}[\mu_2]'_i + \dots \quad (3)$$

and similarly for the other definition matrices.

### Finite Element Analysis

Once the model description is obtained, the next step in the integrated analysis is to generate the equations of motion for the structure. These equations of motion are given by

$$M\ddot{x} + C\dot{x} + Kx = F \quad (4)$$

The task of the structural analysis module is to assemble the mass, damping, and stiffness matrices as well as their sensitivities. While computer codes for finite element analysis abound, few are designed to calculate sensitivities and fewer still can calculate the sensitivities analytically. Because of the importance of fast, accurate sensitivity calculations for the integrated design problem, we chose to develop our own special purpose structural analysis code (called SSA).

The SSA routine has only beam and concentrated mass elements, but it can provide analytical sensitivities of the mass and stiffness matrices for any combination of continuous design variables, such as nodal locations, element properties, and material properties. A lumped mass formulation is employed (resulting in a diagonal mass matrix), and the

stiffness matrix is stored in a banded form. Using the sensitivities of the definition matrices as calculated in Equation (3), the sensitivity of the stiffness matrix with respect to the design variable  $v_i$  is

$$K'_i = \sum_j \sum_k \frac{\partial K}{\partial [X]_{jk}} [X'_i]_{jk} + \sum_j \sum_k \frac{\partial K}{\partial [P]_{jk}} [P'_i]_{jk} + \dots \quad (5)$$

and the mass matrix sensitivities are obtained in the same way.

In COSTAR, the damping matrix  $C$  is never assembled. Instead, the common modal damping approach is used wherein the damping ratio of each mode is specified directly. This implies that the eigenvectors of the undamped problem also diagonalize the damped problem, which is the case when the damping matrix can be expressed in terms of the mass and stiffness as

$$C = M \sum_i a_i (M^{-1}K)^i \quad (6)$$

with arbitrary scalar coefficients  $a_i$  and for any integer values of  $i$ . Rayleigh damping is a special case of Equation (6), with  $i=\{0,1\}$ . With modal damping, the equations of motion become uncoupled and their solution is greatly simplified.

Usually, it is enough to just specify the modal damping ratios and then solve the uncoupled system. In COSTAR, however, it is slightly more complicated. As described below, the response sensitivities are obtained in modal form but without requiring derivatives of the eigenvectors. However, this requires the use of  $C'$ , the sensitivities of the damping matrix. Thus Equation (6) must be differentiated and used to calculate  $C'$ . In the demonstration problem,  $i=1$  was used in Equation (6); this results in damping ratios that are proportional to frequency.

### Eigenvalue Extraction

As mentioned above, the open-loop equations of motion are transformed into modal coordinates (with mass normalization) as

$$\ddot{q}_i + 2\zeta_i \omega_i \dot{q}_i + \omega_i^2 q_i = \phi_i^T F \quad (7)$$

This transformation both uncouples the problem and enables model reduction through modal truncation. At the same time, eigenvalue extraction is often the most computationally expensive part of the open-loop analysis task. Because this step must be performed repeatedly for each new design, the efficiency with which it is performed can determine the practicability of searching for an optimal design. For this reason, we have attempted to perform the eigenvalue extraction as efficiently as possible. To do this, we

have taken advantage of the fact that the eigenvectors from a previous design are usually good approximations to those of the current design.

The existing EIGEN module within IAC is a very efficient eigenvalue extraction code. Nevertheless, its Lanczos algorithm does not benefit from good *a priori* estimates of the eigenvectors. Instead, we have implemented a subspace iteration approach (called *SSI*) that makes successive improvements to a set of starting vectors to eventually converge to the true eigenvectors. The set of equations

$$\begin{aligned}
K \bar{\Phi}_{k+1} &= M \Phi_k \\
\mathcal{K}_{k+1} &= \bar{\Phi}_{k+1}^T K \bar{\Phi}_{k+1} \\
\mathcal{M}_{k+1} &= \bar{\Phi}_{k+1}^T M \bar{\Phi}_{k+1} \\
\mathcal{K}_{k+1} \psi_{k+1} &= \mathcal{M}_{k+1} \psi_{k+1} \Lambda_{k+1} \\
\Phi_{k+1} &= \bar{\Phi}_{k+1} \psi_{k+1}
\end{aligned} \tag{8}$$

are solved for successive values of  $k$  until  $\Phi_k$  converges to the true matrix of eigenvectors. By using the eigenvectors from the previous design as starting vectors for the present design, this convergence is often achieved in only a few iterations.

### Open-Loop Responses

In the COSTAR implementation, the closed-loop transfer functions needed for the objective and constraint evaluations are obtained directly from open-loop transfer functions of the structure via the so-called *Q*-design approach described in the next section. One advantage of this approach is that it does not require the assembly of a state-space (first order) model of the structure. Since the open-loop equations of motion have been transformed into modal coordinates, the open-loop transfer functions can be calculated very efficiently.

In addition to the transfer functions, we also need their sensitivities with respect to the design variables in order to compute the sensitivities of the objective and constraint functions. To determine these sensitivities, it has been common practice to differentiate the modal equations of motion (Equation 7) to form an additional set of equations

$$\ddot{q}_i' + 2\zeta_i \omega_i \dot{q}_i' + \omega_i^2 q_i' = (\phi_i^T F)' - 2(\zeta_i \omega_i)' \dot{q}_i - 2\omega_i \omega_i' q_i \tag{9}$$

that characterize the modal response sensitivities  $q_i'$ . This system has the same frequencies and damping ratios as the original system, but the right-hand side contains not only the forcing function sensitivities but also the responses obtained from solving the original system. In this way, the response sensitivities can be obtained from

$$x' = \Phi'q + \Phi q' \quad (10)$$

Unfortunately, there are well-known difficulties associated with the calculation of eigenvector derivatives [10]. These difficulties are manifested when repeated eigenvalues exist — a common condition in practice.

For COSTAR, we have implemented an approach that appears to offer significant advantages. If the physical coordinates of the original problem in Equation (4) are transformed by some arbitrary constant matrix  $\Theta$ , so that

$$x = \Theta \eta \quad (11)$$

then the equations of motion may be written as

$$\Theta^T M \Theta \ddot{\eta} + \Theta^T C \Theta \dot{\eta} + \Theta^T K \Theta \eta = \Theta^T F \quad (12)$$

By differentiating Equation (12) with respect to the design variables, keeping in mind that the matrix  $\Theta$  is constant, we obtain

$$\Theta^T M \Theta \ddot{\eta}' + \Theta^T C \Theta \dot{\eta}' + \Theta^T K \Theta \eta' = \Theta^T (F' - M' \Theta \ddot{\eta} - C' \Theta \dot{\eta} - K' \Theta \eta) \quad (13)$$

We have not specified the transformation matrix  $\Theta$ ; let us now consider it equal to the eigenvectors of the original system. With this choice, we can see that Equation (13) reduces to

$$\ddot{\eta}_i' + 2\zeta_i \omega_i \dot{\eta}_i' + \omega_i^2 \eta_i' = \phi_i^T (F' - M' \Phi \ddot{\eta} - C' \Phi \dot{\eta} - K' \Phi \eta) \quad (14)$$

and the sensitivities of the physical responses are

$$x' = \Phi \eta' \quad (15)$$

The coordinates  $\eta$  are equal to the modal coordinates  $q$ , but their sensitivities are different.

Comparing Equations (9) and (10) with Equations (14) and (15), the advantages of the latter approach are obvious. In both cases, a second set of equations must be solved in which the original responses appear on the right-hand sides. With the second approach, however, the physical response sensitivities are obtained without computing eigenvector derivatives. Based on our limited experience, this approach seems to work well even when  $\Phi$  contains a truncated set of mode shapes.

## Controls Analysis

A recently developed method for controls synthesis, that is here called *Q-design*, is based on the *Q*-parameterization (or *stable factorization*) theory developed by Youla [11]. With this parameterization, all possible stabilizing controllers and input/output maps can be expressed as functions of a stable parameter *Q*. With this formulation, the closed-loop transfer functions are affine in *Q* — an important property for our purposes.

For a given plant  $P_{yu}$  and nominal controller  $K_{\text{nom}}$ , the stable, co-prime factorization

$$\begin{aligned} P_{yu} &= ND^{-1} = \tilde{D}^{-1}\tilde{N} \\ K_{\text{nom}} &= Y^{-1}X = \tilde{X}\tilde{Y}^{-1} \end{aligned} \quad (16)$$

may be chosen such that

$$\begin{bmatrix} Y & X \\ -\tilde{N} & \tilde{D} \end{bmatrix} \begin{bmatrix} D & -\tilde{X} \\ N & \tilde{Y} \end{bmatrix} = I \quad (17)$$

In that case, the set of all stabilizing controllers is given by

$$K = \{ (Y - Q\tilde{N})^{-1}(X + Q\tilde{D}) \mid Q \text{ stable} \} \quad (18)$$

Furthermore, all achievable closed-loop input/output maps are described in terms of the affine *Q* parameter via

$$H_{zw} = T_1 + T_2QT_3 \quad (19)$$

where the nominal system is characterized by

$$\begin{aligned} T_1 &= P_{zw} - P_{zu}DXP_{yw} = H_{zw}|_{Q=0} \\ T_2 &= -P_{zu}D = H_{zv} \\ T_3 &= \tilde{D}P_{yw} = H_{ew} \end{aligned} \quad (20)$$

The *Q* parameter may be thought of as a tuning parameter for the nominal controller. Figure 3 depicts its connection to the nominal controller. Here *P* represents the plant and  $K_{\text{nom}}$  represents the nominal controller. The plant has control inputs *u*, exogenous inputs *w*, regulated outputs *z*, and measured outputs *y*. The exogenous inputs include signals such as commands, disturbances, and sensor noise. The regulated outputs are signals that the designer has chosen to regulate, and that reflect the performance of the system.

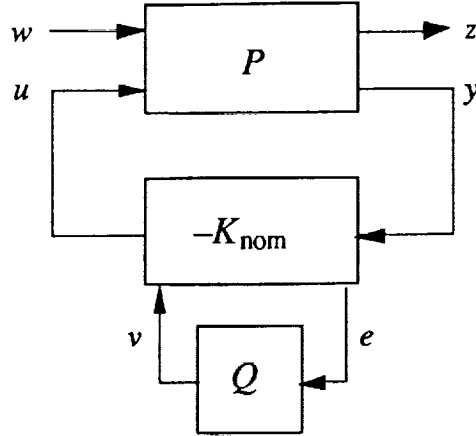


Figure 3: Nominal controller modified by  $Q$ .

$Q$  is connected to the nominal controller in such a manner (according to the equations above) that it sees no feedback. That is, the transfer function from  $v$  to  $e$  is zero. Thus, if  $Q$  is stable, it cannot affect the stability of the closed-loop system. By allowing  $Q$  to range over all stable transfer functions, the combination of the nominal controller and  $Q$  span the space of all possible stabilizing compensators.

This  $Q$ -parameterization theory can be used in a design procedure by searching for a suitable  $Q$  parameter within a finite subset of the stable transfer functions. This method has been implemented by Boyd [12] in a computer code called *QDES*. The  $Q$  parameter is represented by

$$Q = \sum_i v_i Q_i \quad (21)$$

a linear combination of a finite set of fixed, stable maps  $Q_i$ . Thus  $Q$  is restricted to a set of finite impulse response (FIR) filters. In *QDES*, numerical optimization is then used to search for a set of design variables  $v$  that minimize the objective function while satisfying the constraints.

The  $Q$ -design approach offers several attractive features. It allows the user to directly specify an objective function and strict equality and inequality constraints on a wide variety of closed-loop system characteristics. (See Table 2.) In addition, it is capable of producing a wide variety of controllers, including those obtainable with LQG [15] and  $H_\infty$  [16] methods as subsets.

### **Objective Functions**

- Transfer function 2-norm (LQG)
- Power spectral density of a transfer function at specified frequencies
- Overshoot and undershoot for a step input
- Stability margins
- Infinity-norm of impulse and step responses
- Transfer function infinity-norm (H-Infinity)

### **Constraints**

- Limits on impulse and step responses of states and controls
- Limits on step response overshoot and undershoot
- Limits on transfer function infinity-norm
- Limits on step and impulse response infinity-norms
- Limits on stability margins

**Table 2: Sample QDES control specifications.**

What makes this approach tractable is the fact that, excluding the structural design variables, the resulting optimization problem is a convex one. This is a great benefit; even though the number of design variables may be very large, the problem remains relatively simple and a solution will be found if it exists.

Admittedly,  $Q$ -design has some drawbacks. Because it is based on numerical optimization, it can require a significant amount of computation. In addition, the resulting controllers are of very high order. Nevertheless, the method does show promise. In our experience with it so far, the computational effort has been large but not prohibitive, and the high order controllers have been amenable to reduction techniques.

### **Demonstration Problem**

A representative problem was selected on which to demonstrate the integrated design methods and software developed for this task. This example structure, known as the Earth Pointing System (EPS) [13] is shown in Figure 4. It is derived from the Ford Earth Observation Sciences geostationary platform and consists of a truss-type bus with two flexible antennas. The bus is approximately 25 meters in length and the antennas are 15 and 7.5 meters in diameter.

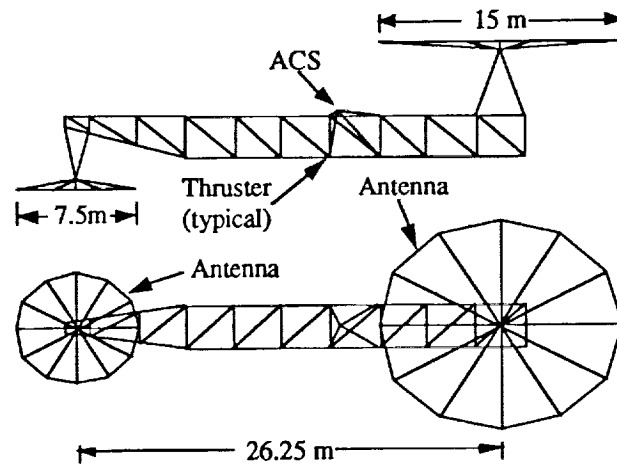


**Figure 4: The Baseline EPS Structural Model**

The total mass of the baseline structure is 1027.95 kg, including 150 kg of actuator mass and 548.32 kg of nonstructural mass on the antennas. The truss has a 3.0 meter cross section and consists of 135 graphite/epoxy tubes. The first flexible mode of the structure mostly involves rotation of the antennas and has a frequency of 0.24 Hz. Shapes and frequencies of the first 16 flexible normal modes are shown in Appendix A. Many of these modes involve local deflections within the antennas with insignificant motion of the truss.

The design problem considered here is one of active vibration suppression. The flexible structure has no articulated elements; the controller is required to regulate the structure about some nominal attitude while enhancing the stability of the rigid body modes. A set of reaction wheel actuators is located near the center of gravity of the baseline system and is used to control the pointing errors of the antennas due to the flexible response of the structure. Angular rate sensors are colocated with the reaction wheel actuators, and linear accelerometers are included at the center of each antenna.

Dynamic excitation of the structure is considered from a thruster located on the main bus module. To expedite the present study, no other loads were considered. The methods developed, however, do not restrict the number or characteristics of the external loads. In fact, satisfactory practical designs would seem to require many load cases, in both the time and the frequency domains.

A total of 19 structural design variables were chosen for the EPS structure, including bar radii for various groups of bars, the width and depth of the truss at several points along its length, and the size and orientation of the antenna supports. These design vari-



ables are described in Table 3. Figure 5 shows an example of the structure for which arbitrary values have been chosen for each design variable.

Name	Description	Baseline Value
C_WIDTH	Width of the truss at its center.	3.0 m
C_DEPTH	Depth of the truss at its center.	3.0 m
L_WIDTH	Width of the truss at the large antenna end.	3.0 m
L_DEPTH	Depth of the truss at the large antenna end.	3.0 m
SMALL_Y_1	Value of the y-coordinate of the truss at the end nearest and on the same side as the small antenna.	1.0 m
SMALL_Y_2	Value of the y-coordinate of the truss at the end nearest and on the opposite side as the small antenna.	1.5 m
S_DEPTH	Depth of the truss at the small antenna end.	0.5 m
ALPHA	Angle between the truss axis and the plane of the antennas.	0.0
LONGERON_R	Radius of the longerons.	0.0255 m
BATTEN_R	Radius of the battens.	0.0255 m
DIAG_EXT_R	Radius of the external diagonals.	0.0255 m
DIAG_INT_R	Radius of the internal diagonals.	0.0255 m
L_SUP_R	Radius of the large antenna supports.	0.0255 m
S_SUP_R	Radius of the small antenna supports.	0.0255 m
ACT_SUP_R	Radius of the actuator supports.	0.0255 m
ACT_MASS	Actuator mass.	150.0 kg

Table 3: Design variables for the EPS structure.

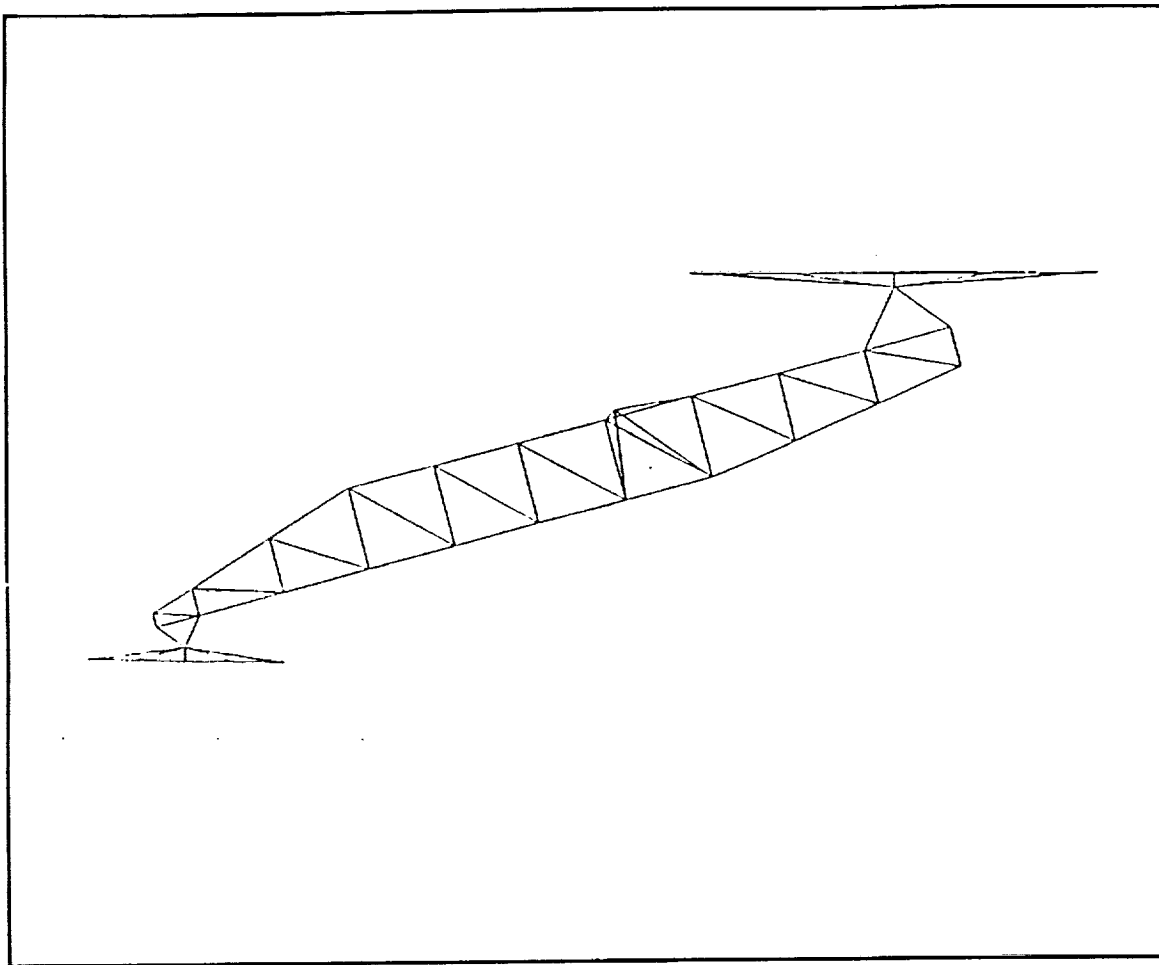


**Figure 5: Structure with arbitrary changes in the design variables.**

The EPS equations of motion that were used for the control design contained the first 16 flexible modes, ranging from 0.24 Hz to 3.53 Hz. A sample frequency of 20 Hz was used, with 20  $Q$  taps and 500 samples. The sample rate is sufficient to capture at least 5 points in every cycle of the highest frequency mode, and the 500 samples used for the open-loop impulse responses is sufficient to capture 6 full cycles of the lowest frequency.

Figure 6 illustrates the locations in the baseline model relevant to the control design.

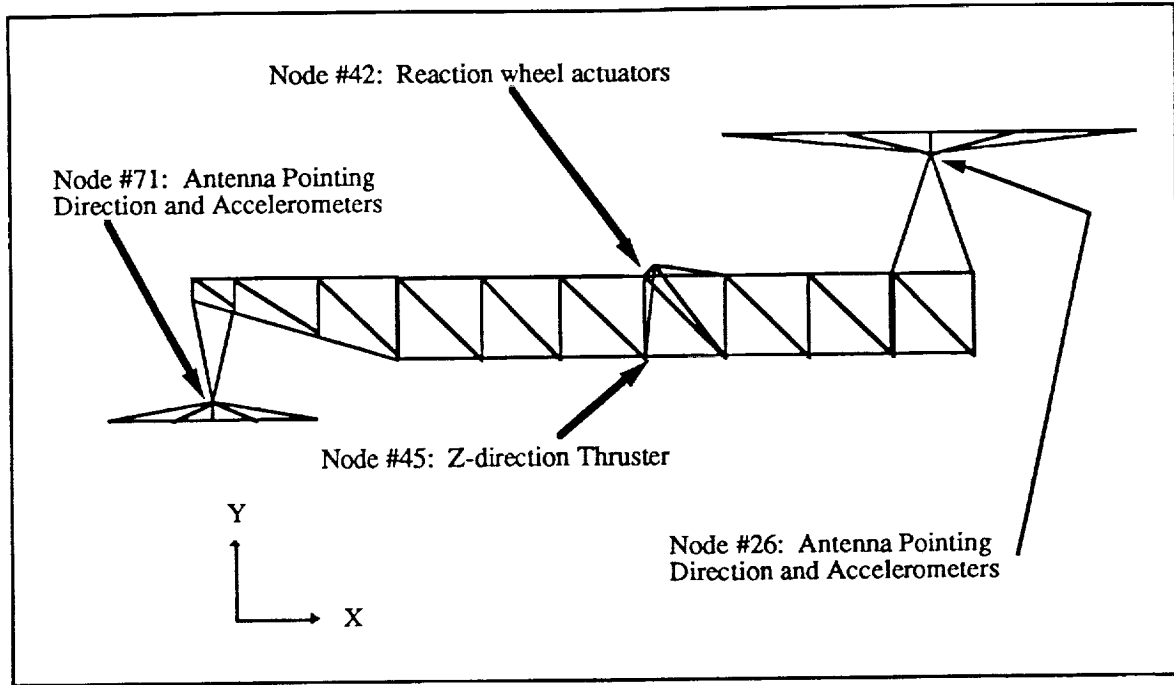


**Figure 6: The baseline EPS structure.**

Rotations about the  $x$ ,  $y$  and  $z$  axes are designated as  $\theta$ ,  $\phi$ , and  $\psi$ , respectively. The actuators are reaction wheels located at node #42. The torques exerted by the actuators are designated as  $f_{\theta 42}$ ,  $f_{\phi 42}$ , and  $f_{\psi 42}$ . A thruster, which represents a disturbance for the control task, is located at node #45 and exerts a thrust  $f_{z45}$ , in the positive  $z$ -direction. The measured outputs are the three components of angular rate at node #42 and the linear accelerations in the  $x$  and  $z$ -directions at nodes #26 and #71. The control objective is to regulate the antenna angles  $\theta_{26}$ ,  $\psi_{26}$ ,  $\theta_{71}$ , and  $\psi_{71}$  using the reaction wheel actuators.

The initial system configuration provided by the structural model consists of 1 exogenous input, 3 controller inputs, 4 regulated outputs, and 7 measured outputs. This configuration is depicted in Figure 7.

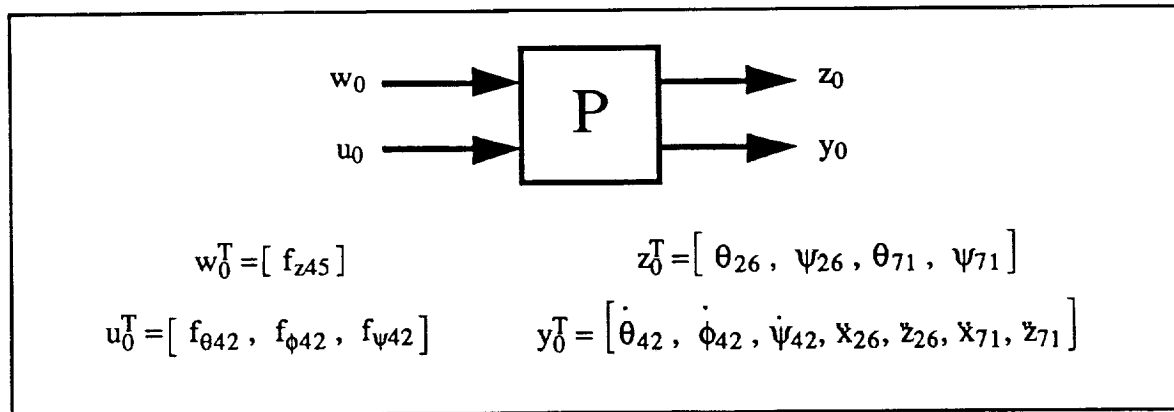


**Figure 7: The original plant defined by the structural model.**

To accommodate the design of a robust system, several additional inputs and outputs were added to the system. As shown in Figure 8, actuator noise and sensor noise were added. Also, the exogenous output was augmented with the noisy actuator signal and the angular rates measured at the reaction wheels. This configuration now allows for a wide variety of control specifications, including robustness and noise sensitivity.

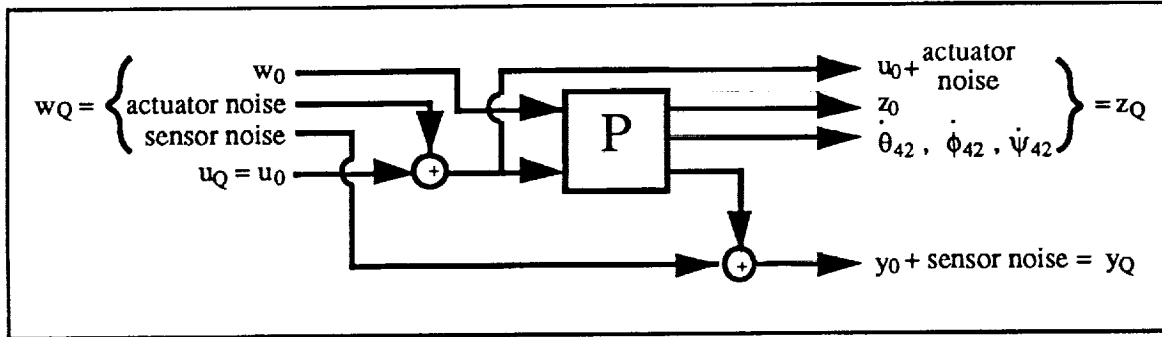


Figure 8: Augmented plant.

## Findings

The COSTAR implementation of the integrated design method described previously was applied to the EPS design problem. This was done in two ways: (1) with all the structural design variables held fixed, and (2) with all but one of the structural design variables held fixed. The first analysis amounts to an optimal control design for the baseline structure, which is useful for evaluating the  $Q$ -design methodology. The second analysis is an integrated design optimization of the controlled EPS structure. Because the analytical sensitivity computations were incompletely implemented in COSTAR at the time, the latter analysis considered only a single concurrent structural design variable. Although this is a severe limitation in the optimization problem, the integrated design capability of COSTAR is nevertheless demonstrated adequately.

### Optimal Control Using $Q$ -Design

By fixing the structural design variables, COSTAR is essentially identical to the QDES control design code. The control design variables shown in Equation (21) are adjusted to minimize the objective function while satisfying the constraints. This control design is for a specific disturbance — a 100 N-s impulsive force in the  $z$ -direction by the thruster at node #45.

The objective function chosen for this demonstration contained control effort, pointing error, and stability margin components. Specifically, this objective was calculated as the sum of  $10^3$  times the mean square torque,  $10^{16}$  times the mean square pointing error, and  $10^4$  times the inverse of the minimum Nyquist distance†. (All quantities are measured in SI units.) These costs were chosen for a disturbance environment where the ratio of thrust disturbance to sensor noise is approximately 10,000.

Constraints were applied to the antenna pointing error, the actuator torque levels, and robustness to actuator noise. The maximum allowable pointing error of either antenna was  $0.01^\circ$ . The torque applied by the reaction wheel actuators was limited to at most 1000 N·m. The minimum Nyquist distance was required to be at least  $0.5 \text{ s}^{-1}$ .

These objective and constraint functions, along with the impulse responses of the baseline system, were given as input to QDES. The result was an optimal controller that minimized the costs without violating the imposed constraints. As mentioned earlier, QDES often results in high order controllers, and this design was no exception. For the 36 state baseline system, QDES found a 146 state controller. It was demonstrated using the controller order reduction technique of frequency weighted internal balancing [14], that the controller could be reduced to 30th order with minimal impact upon performance.

To the closed-loop system thus obtained, a 1 N·s impulsive disturbance in the z-direction was applied by the thruster at node #45. This is precisely the disturbance for which the controller was designed, except that its magnitude is scaled by 100. The resulting response and the response of the open-loop system are depicted in Figures 9-18.

Figure 9 depicts the pointing error about the x-axis at the small antenna,  $\theta_{71}$ , for this impulsive disturbance. Recall that the control specifications included a constraint on pointing error of  $0.01^\circ$  for a 100 N·s impulsive input. This translates into a  $1.7 \times 10^{-6}$  radian limit for a unit impulse, which is shown in the figure. One can see that the open-loop response clearly violates this constraint. It has a peak response of  $-6.5 \times 10^{-6}$  radians. On the other hand, the closed-loop response goes right up to the constraint in about 0.5 seconds, but never violates the constraint. Of the four pointing angles,  $\theta_{71}$  is the most sensitive to the thruster disturbance. The other pointing angle responses, shown in Figures 10-12, do not violate the pointing constraints even for the open-loop case. The response of  $\psi_{26}$ , the pointing error about the z-axis depicted in Figure 12, is roughly three orders of magnitude less than that of  $\theta_{71}$ .

Figures 13-15 illustrate the effect of the impulse on the angular rates measured at the actuators. The closed-loop response exhibits greatly improved dynamic behavior. No constraints were imposed upon these angular rates.

Finally, Figures 16-18 depict the response of the actuators to the impulsive disturbance. The actuators were constrained to have a 10 N·m peak torque level. For the baseline structure, however, none of the actuators approached this limit. A peak torque level of approximately 2 N·m was seen in actuators  $f_{\theta 42}$  and  $f_{\phi 42}$ . During the combined optimization, however, it is entirely possible that the structure might evolve into one where this peak torque limit could be reached. Placing this limit prevents the optimization procedure from designing a system that would require excessive actuator authority.

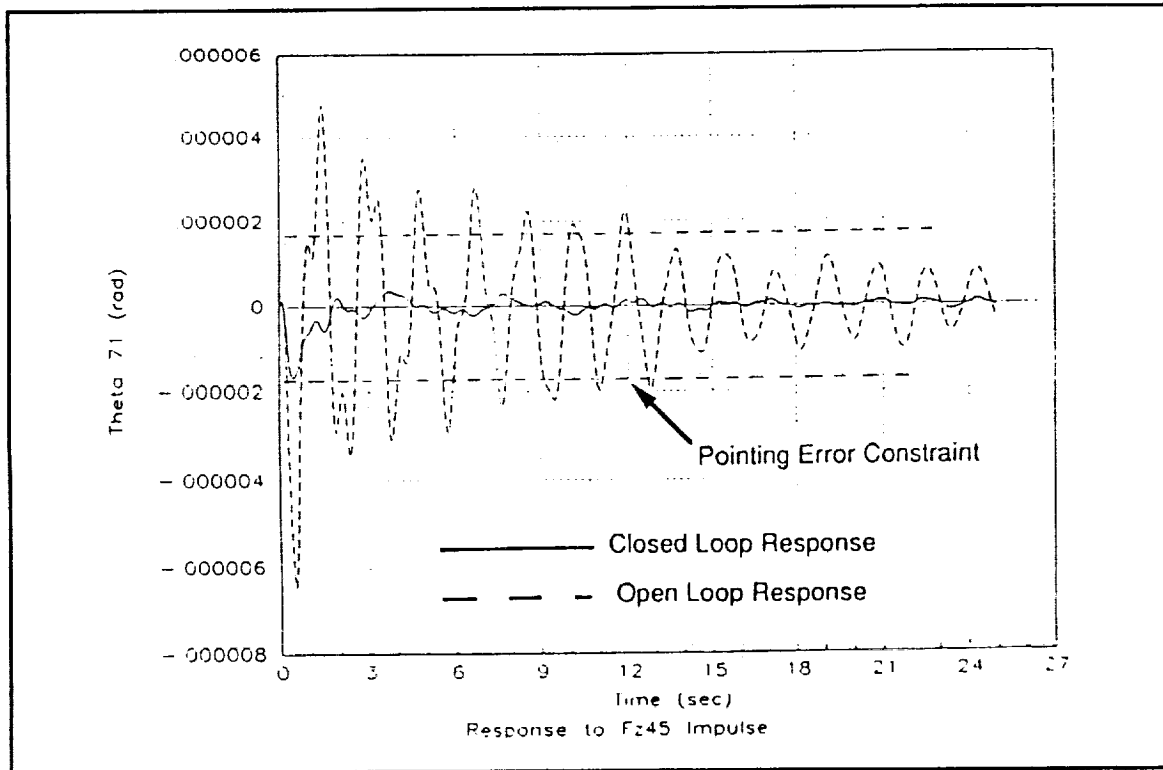


Figure 9: Response of  $\theta_{71}$  to a unit  $f_{z45}$  impulse.

† The *minimum Nyquist distance* is the minimum distance between the Nyquist curve and the “-1 point” (the point of instability) in the complex plane.

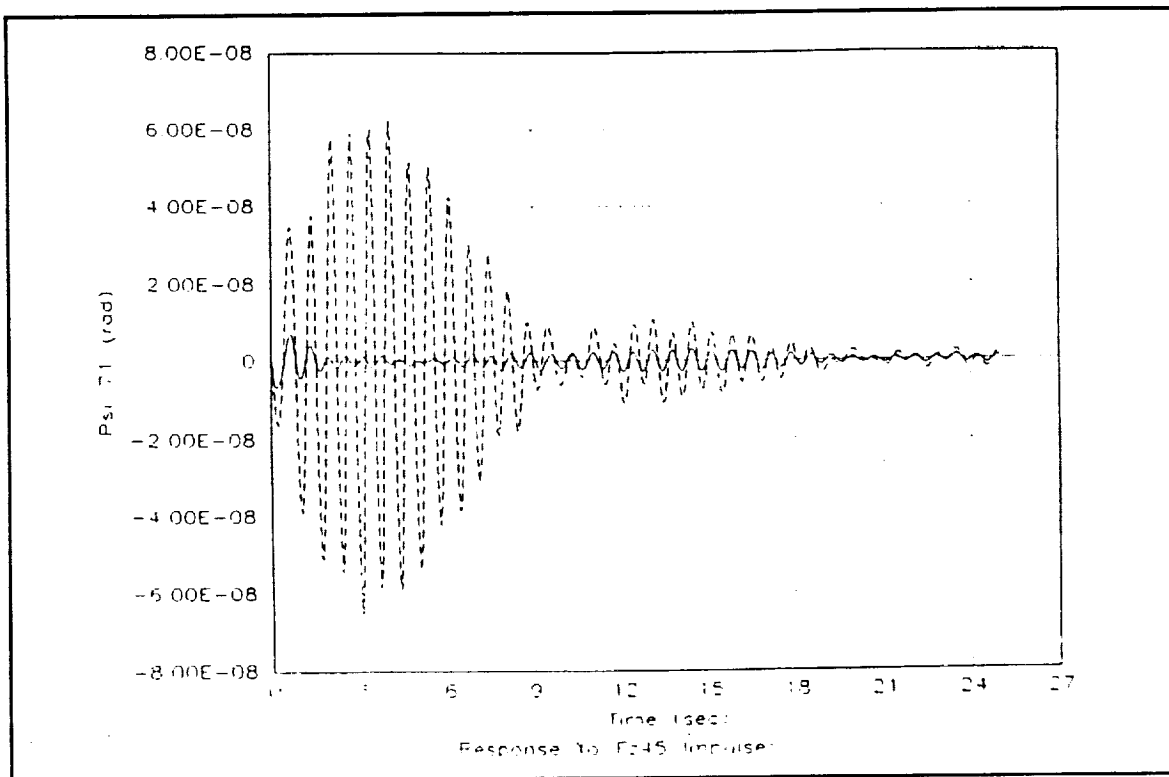


Figure 10: Response of  $\psi_{71}$  to a unit  $f_{245}$  impulse.

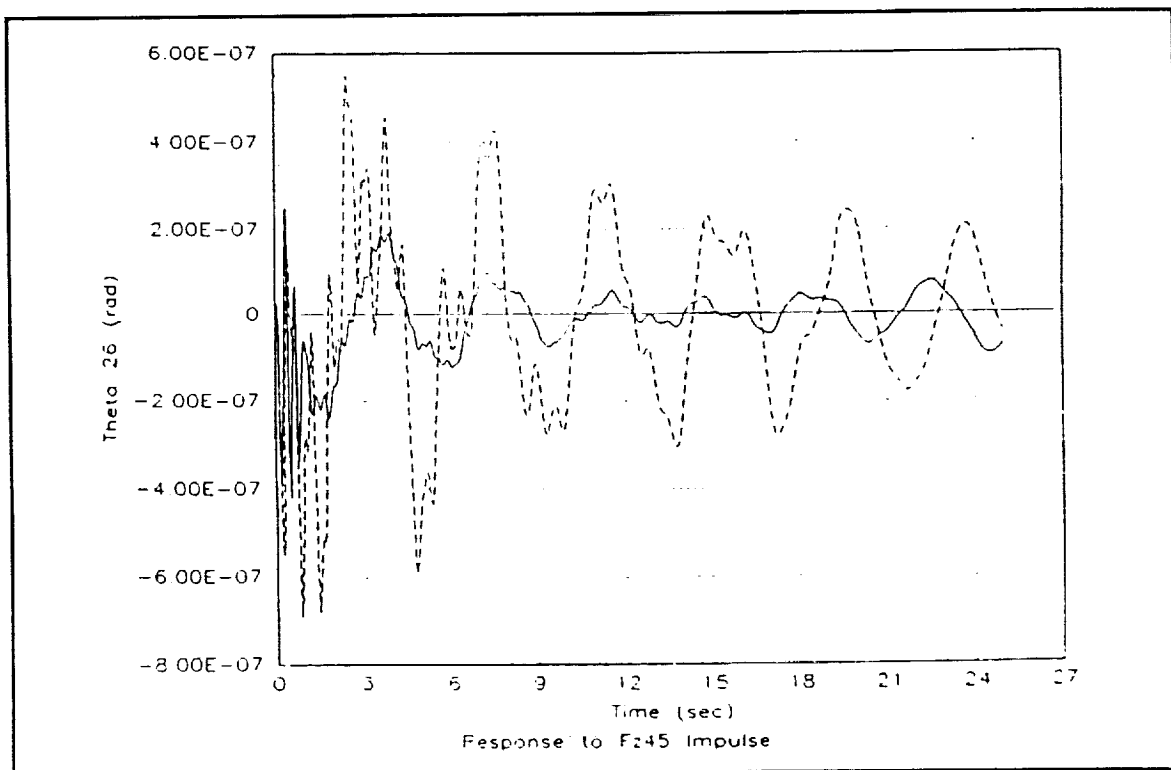


Figure 11: Response of  $\theta_{26}$  to a unit  $f_{245}$  impulse.

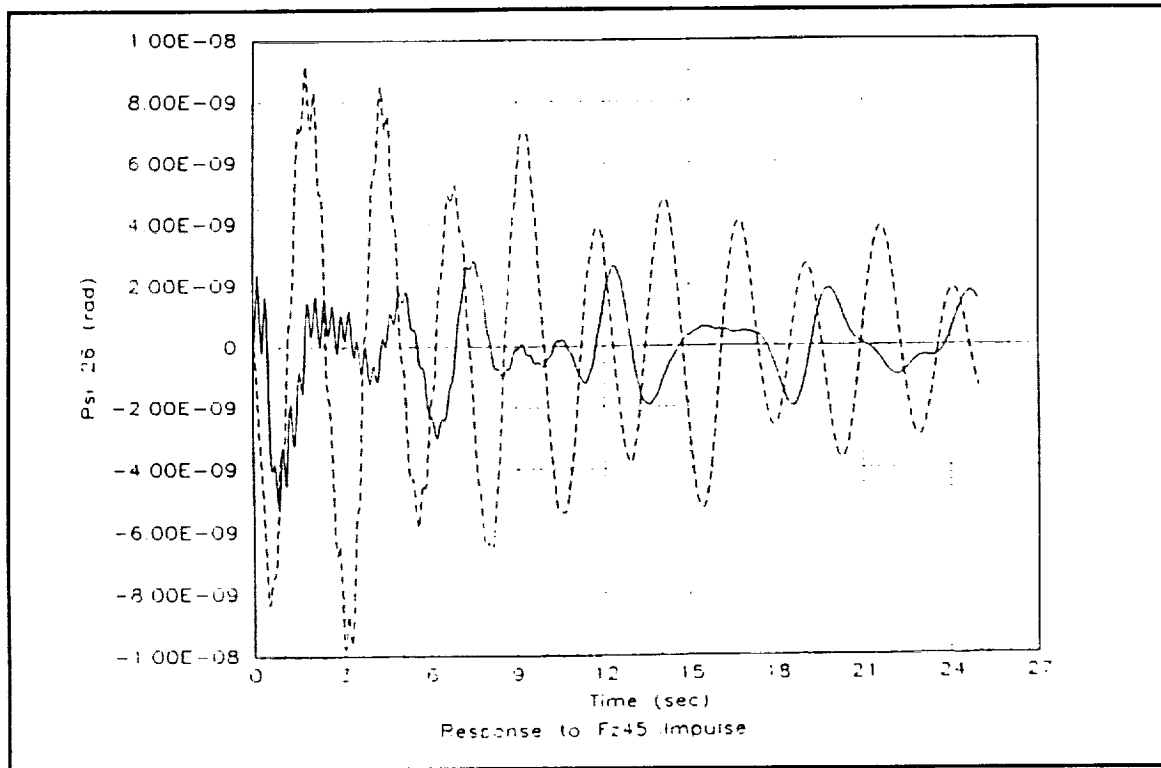


Figure 12: Response of  $\psi_{26}$  to a unit  $f_{z45}$  impulse.

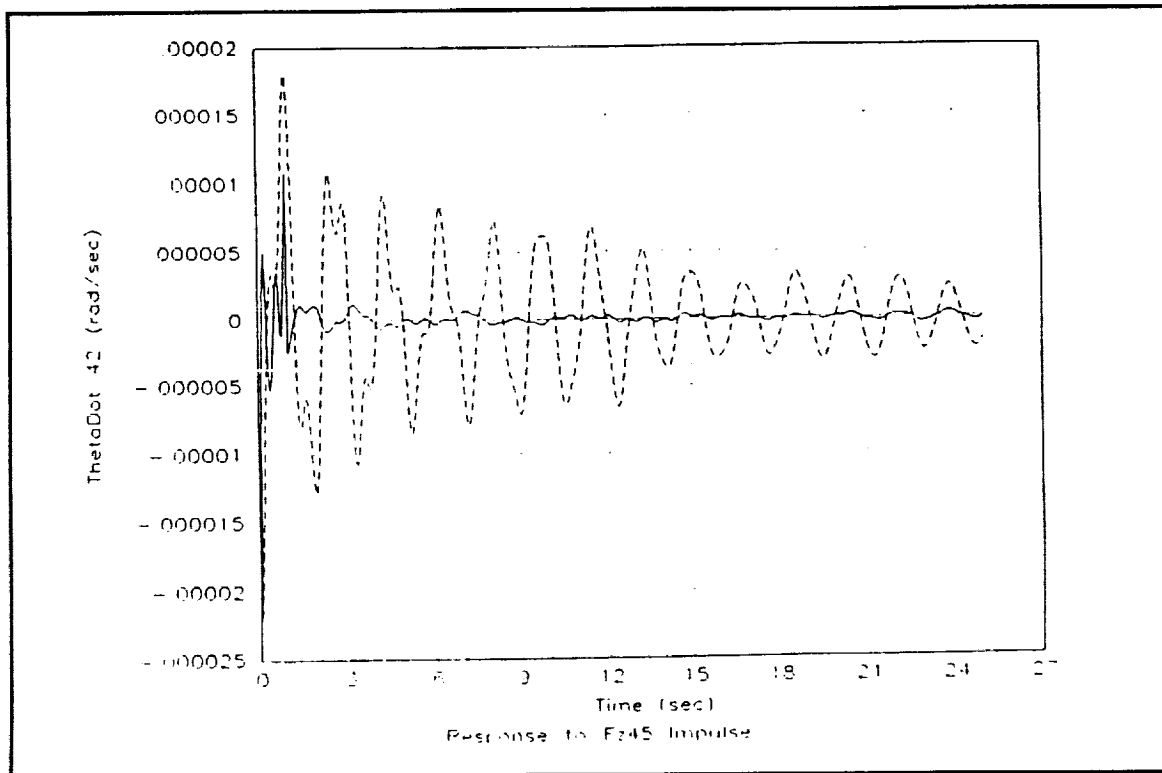
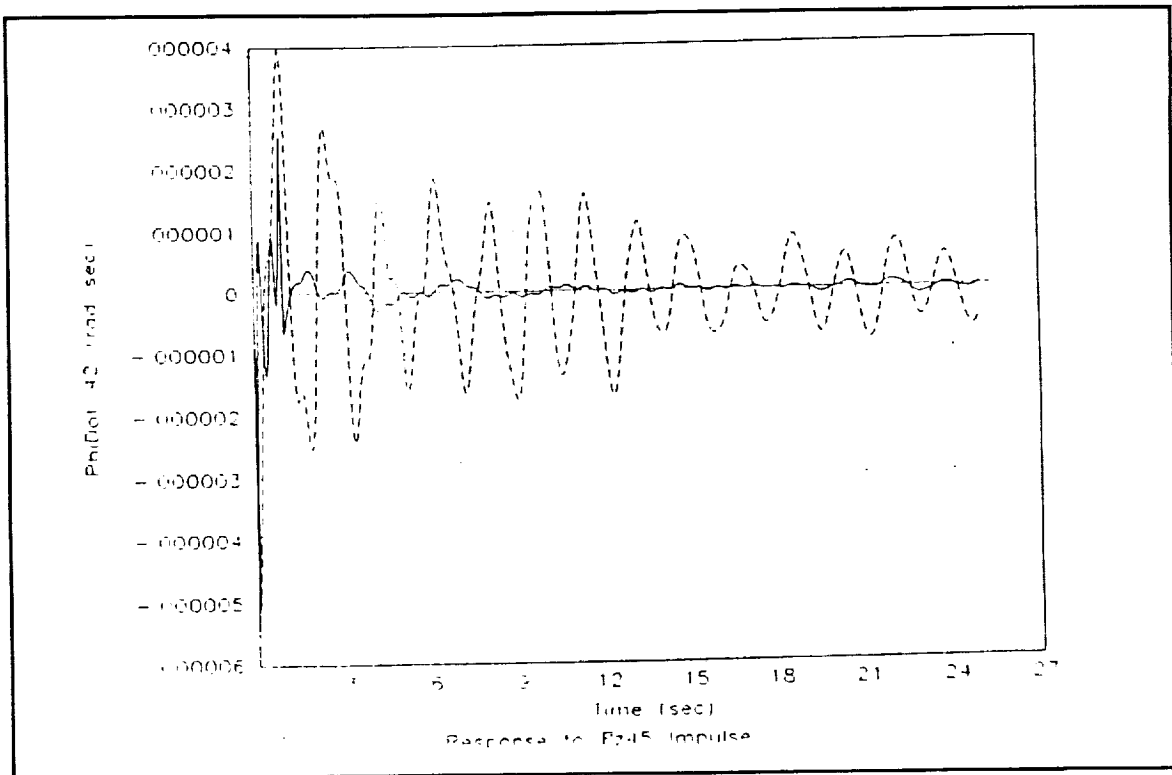
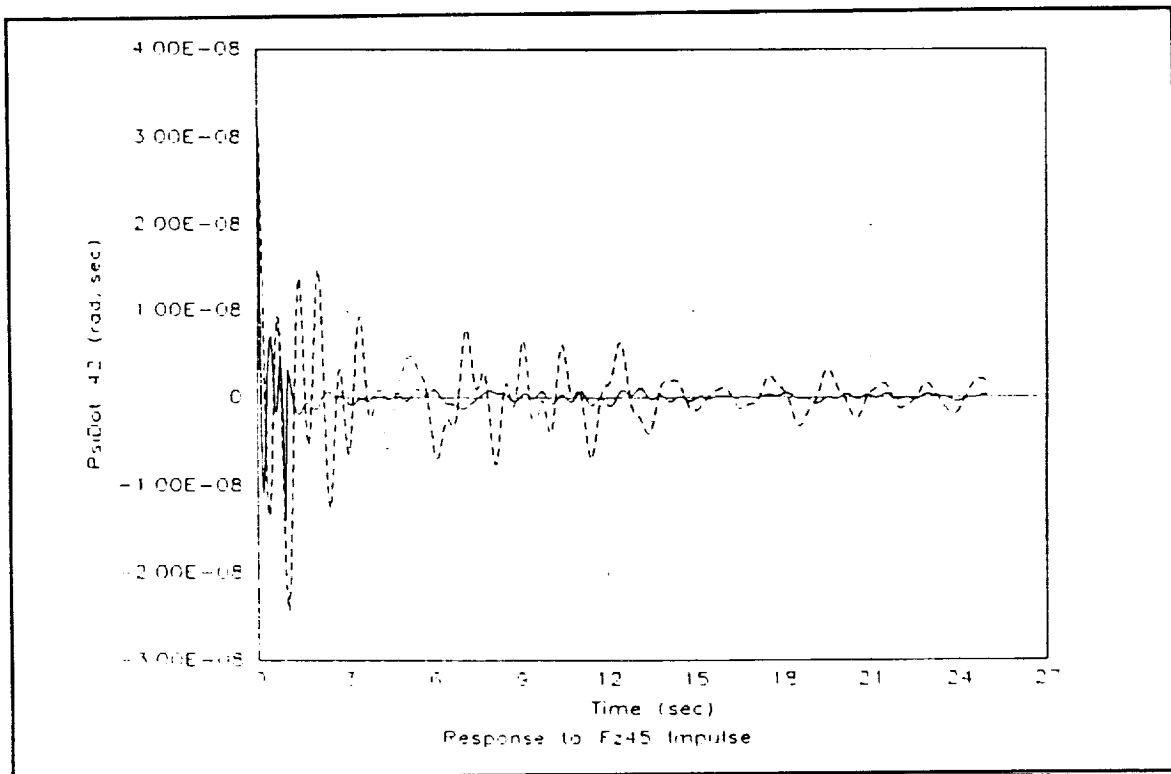


Figure 13: Response of  $\theta_{42}$  rate to a unit  $f_{z45}$  impulse.





**Figure 14: Response of  $\phi_{42}$  to a unit  $f_{z45}$  impulse.**



**Figure 15: Response of  $\psi_{42}$  to a unit  $f_{z45}$  impulse.**

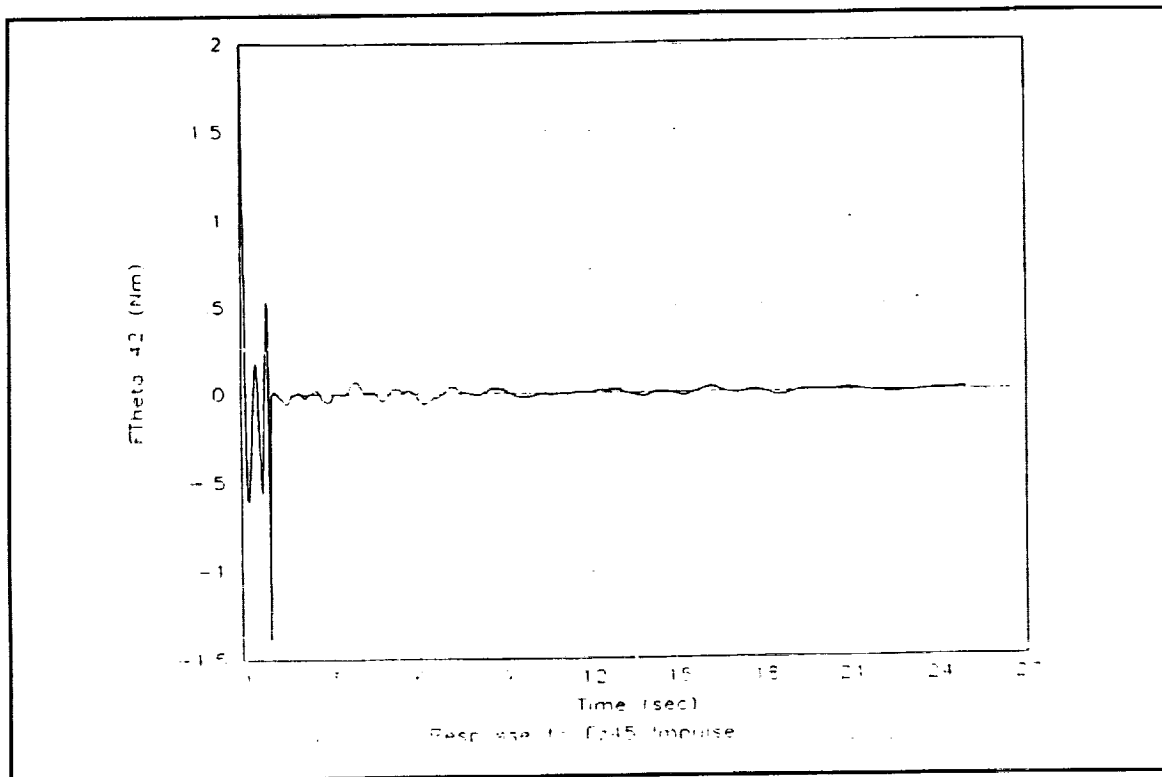


Figure 16: Response of  $f_{\theta 42}$  to a unit  $f_{z45}$  impulse.

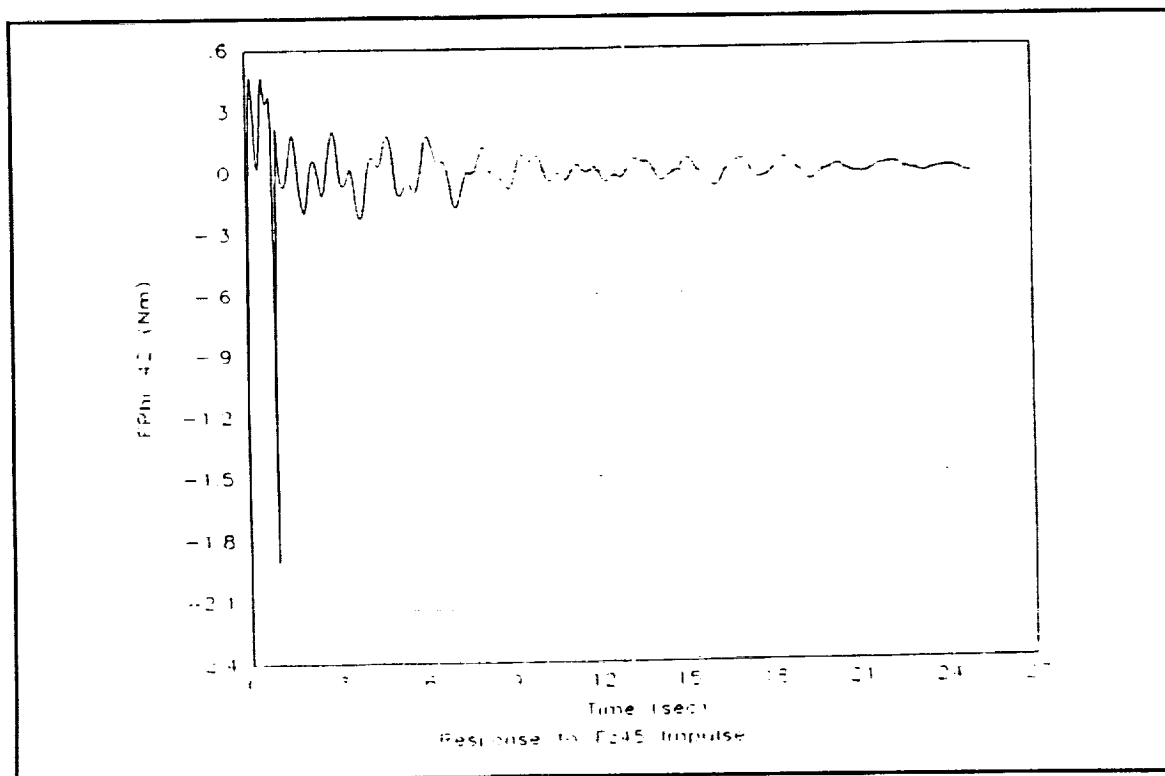


Figure 17: Response of  $f_{\phi 42}$  to a unit  $f_{z45}$  impulse.

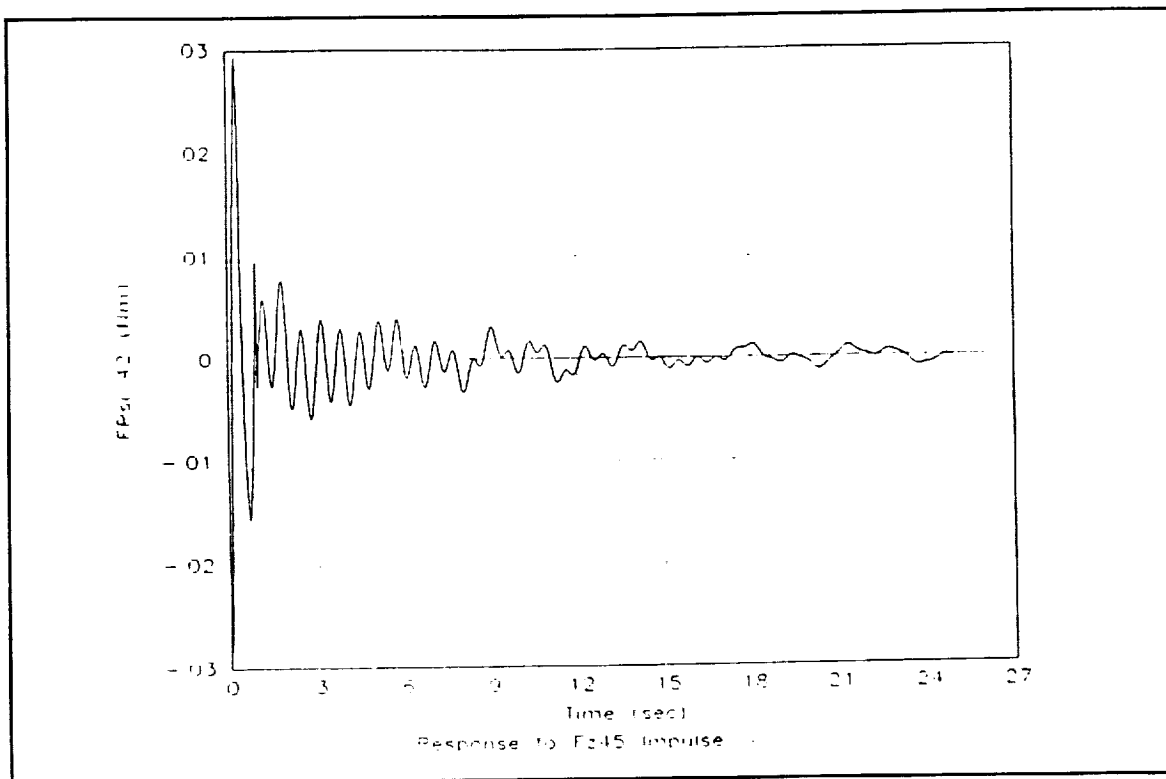


Figure 18: Response of  $f_{y42}$  to a unit  $f_{z45}$  impulse.

### Combined Optimization

The results presented above pertain to a COSTAR optimization in which only control design variables were considered. By extending that analysis to include structural design variables, the integrated design capability of COSTAR can be demonstrated. As mentioned previously, the analytical sensitivity computations were incompletely implemented in COSTAR, forcing us to consider only one structural design variable at a time. We performed two such analyses, including the width and depth of the center section of the EPS truss. (These are the variables C\_WIDTH and C\_DEPTH described in Table 3.)

For this integrated design problem, the objective function described in the previous section was augmented to include a term proportional to the total mass of the structure. In many cases, this mass term may adequately account for the cost of the materials and the cost of transporting the structure to orbit. It cannot account, however, for many other costs such as manufacturing and assembling the structure. As with any structural optimization procedure, the results are only as good as the objective function. Although this demonstration used a very simple objective function, the only objective function limitation in COSTAR is that it must be twice-continuously differentiable.

In addition to the control constraints described previously, simple side constraints were applied to the structural design variables. These constraints specified commonsense

restrictions such as that the truss cross section must have a reasonable width and depth. Far more complicated constraints (on stresses, strains, etc.) could be included if desired.

In Figure 19, the objective value is shown as a function of the center section truss depth. Each point on the curve represents a particular design analyzed by COSTAR in which an optimal control design is obtained. The baseline EPS structure has a depth of 3.0 m; the figure shows that its optimum value (for the objective and constraint functions specified and for the particular finite-dimensional space from which  $Q$  is chosen) is approximately 2.6 m. Significant contributions to the objective function value come from the total mass and mean square pointing error terms. Because the mass varies by only 7% over the range of truss widths shown, it does not play a significant role in determining the location of the optimal design. Nevertheless, incorporation of the structural design variable clearly has an important effect on the closed-loop behavior and on the performance of the resulting design.

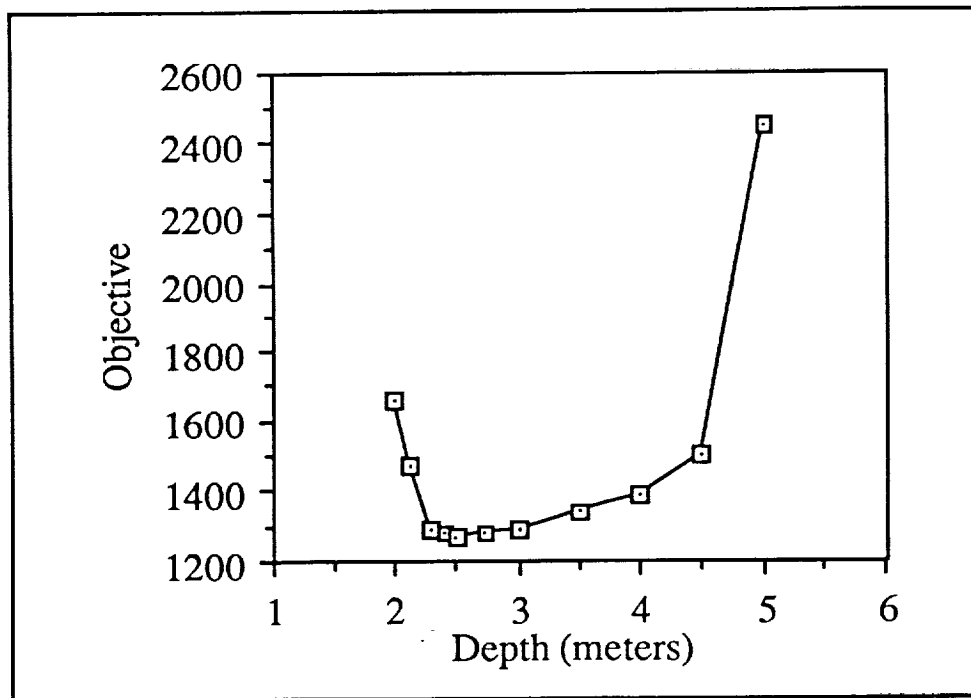
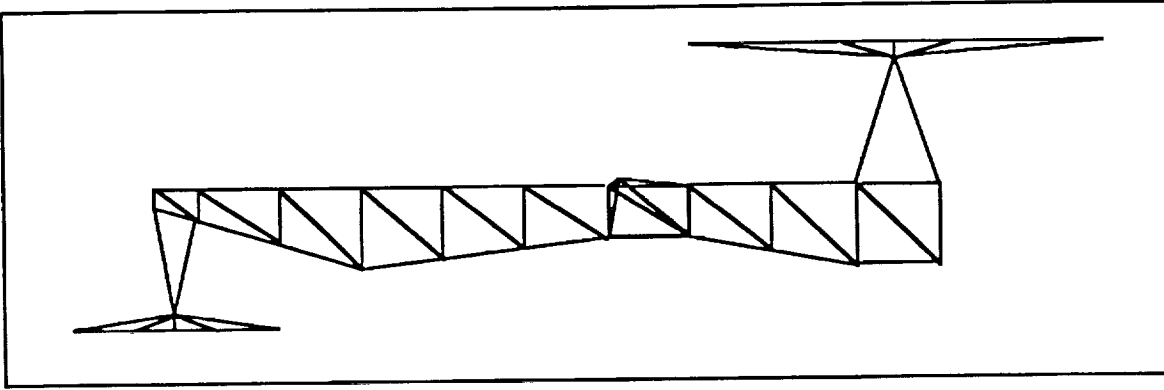


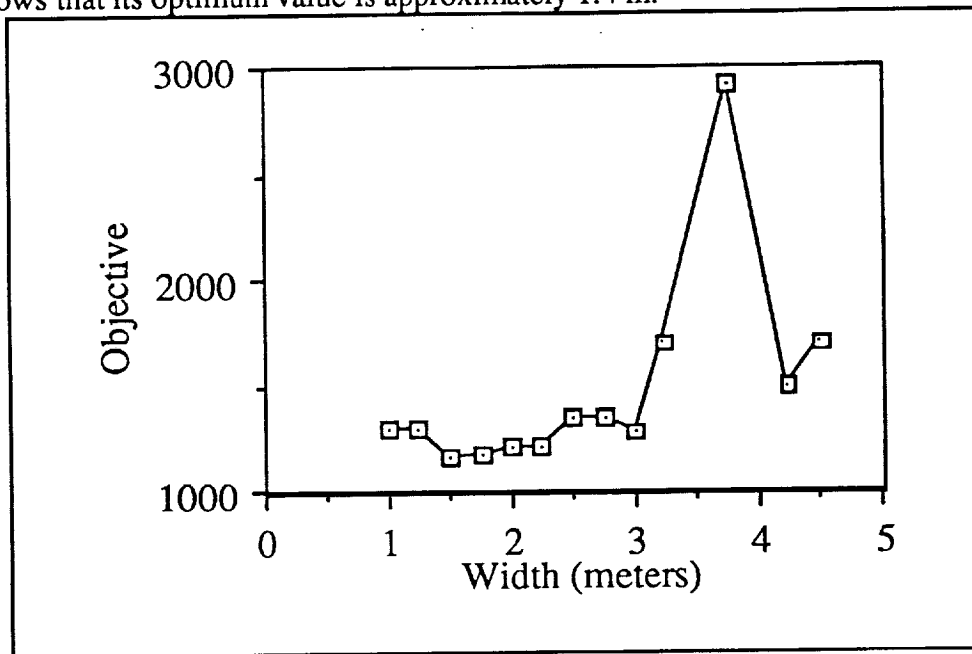
Figure 19: Objective vs. truss depth.

Figure 20 shows the combined control/structure optimum configuration obtained. At 2.6 m, the center section depth has decreased from the baseline EPS design — a change that significantly decreases the bending stiffness of the truss. This narrowing of the center section obviously decreases the structural cost (total mass) slightly, but it also decreases the combined costs associated with control energy and performance.



**Figure 20: Optimized structure considering control and truss width.**

A similar analysis was performed with the center section width, rather than depth, as the structural design variable. A plot of the objective value versus this width is shown in Figure 21. Here again, each point represents a system for which an optimal controller has been designed with COSTAR. The baseline EPS structure has a depth of 3.0 m; the figure shows that its optimum value is approximately 1.4 m.



**Figure 21: Objective vs. truss width.**

Because the optimal control problem is convex, we know that each point in Figure 21 represents a globally optimal design for that particular structure. As the figure demonstrates, however, the optimization problem is no longer convex when structural design variables are introduced. Several local minima are seen to exist. Clearly, finding a global optimum is not generally assured for the combined problem.

Figure 22 shows the combined control/structure optimum configuration considering the truss width structural variable. Note that, as with the center section depth, the optimum center section width is also less than that of the baseline EPS structure — again a change that significantly decreases the bending stiffness of the structure.

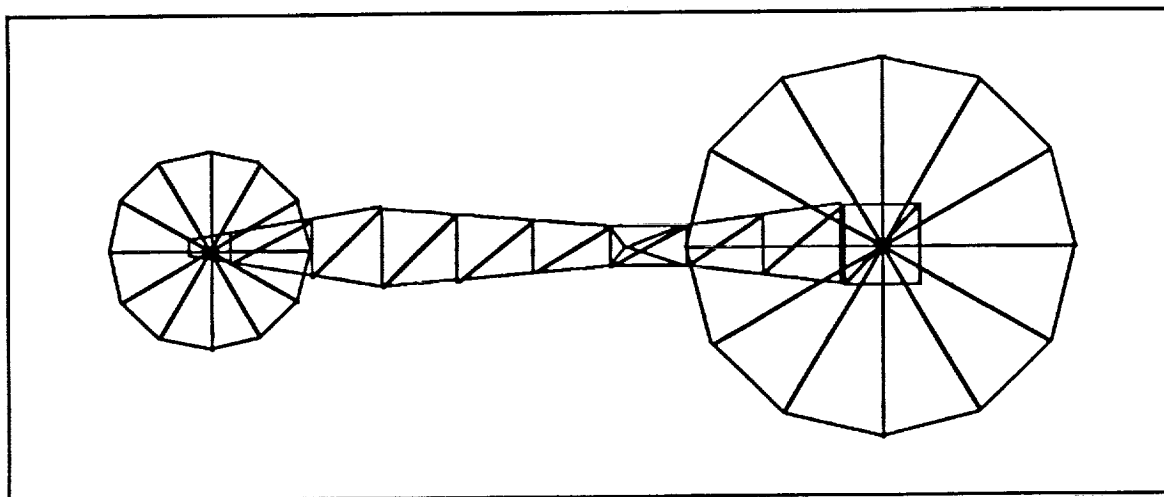


Figure 22: Optimized Structure Considering Control and Structural Depth

## Conclusions

In conducting a simultaneous optimization of both structural and control parameters, it is possible to investigate design configurations which a separate control and structure optimization would miss. Thus, the overall approach to combined control/structure optimization presented in this report holds promise for generating non-intuitive optimal designs. In particular, the optimization of the EPS structure described in this report found that it was optimal to decrease the size of the center truss section. This represents a reduction in structural stiffness - a result which might run counter to intuition.

In the process of developing this combined control/structure optimization, a method for determining structural sensitivities was developed. This method of analytically calculating structural sensitivities represents a significant improvement over other methods involving either finite differencing or the differentiation of eigenvectors.

The control aspect of the optimization was accomplished using the relatively new control synthesis tool called *Q-design*. As implemented by the program *QDES*, this design method has been demonstrated to work well in the combined optimization context. It has proven to be a very flexible tool for making control design specifications and synthesizing controllers that meet these specifications.

With this increased flexibility also comes increased computational cost. In addition, controllers developed using Q-design tend to be of very high order — much higher than that of the systems they are controlling. On the other hand, it has been demonstrated that the controller order reduction technique of frequency weighted balancing can greatly reduce controller order. Moreover, the use of Q-design in the combined optimization does not preclude the use of other control design tools for the optimized structure; the benefits of Q-design would have then already been exploited by designing a system for which it is theoretically possible to achieve the desired performance.

While optimization over the control design variables is a convex problem, it is not convex over the structural parameters. Consequently, the combined control/structure optimization will most likely have local minima, and the process of attempting to find a design that achieves a global minimum will require multiple starting points.

### **Areas for Future Research**

At this point, the COSTAR optimization procedure requires a great deal of supervision and designer input. This is related primarily to facilitating communication between the various software components. One of the primary goals of future work would be to streamline the optimization procedure. Ideally, once the structural model and its design variables have been defined, and once the objective and constraint functions have been specified, the optimizer should be able to run "hands free" until an optimal design is found. This streamlining of COSTAR would also facilitate the inclusion of a larger number of structural design variables. Present designs have only been optimized over one structural variable and all control variables.

Some of the subprocesses in the optimization procedure have room for much improvement. In particular, the implementation of analytic design sensitivity computations should be completed in order to facilitate the inclusion of a larger number of structural design variables. Another area for research is the eigenvalue extraction method, which might make better use of the eigenvalues calculated for previous structures, since from one design iteration to the next the structure does not change a great deal. The effects of modal truncation, as they relate to this simultaneous optimization problem, should be studied further.

Finally, it would be advantageous to develop a means of reducing the computation time associated with the control part of the optimization. Some research has been done in this area by Kosut and Kabuli, and is included as Appendix B in this report. This approach involves a pre-filtering of the Q-filter in an attempt to reduce the number of taps necessary to obtain a good control design. Another approach would be to incorporate a

nominal controller for the baseline system. This would reduce the number of samples required to characterize the impulse responses, and would also reduce the number of taps required in the  $Q$ -filter.

## References

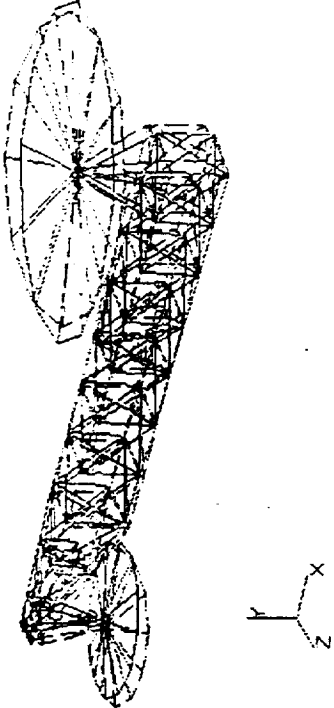
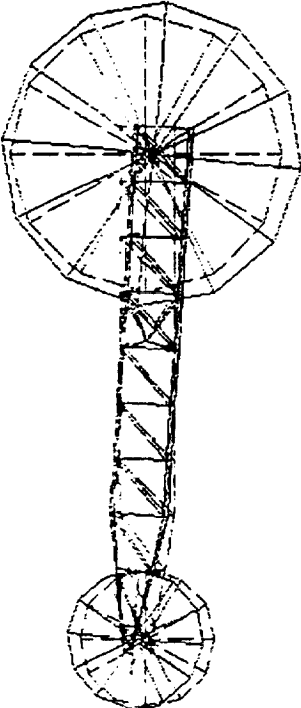
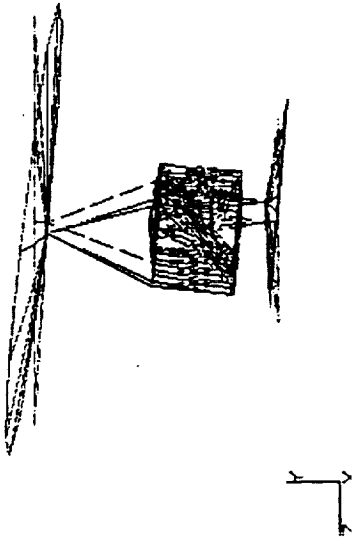
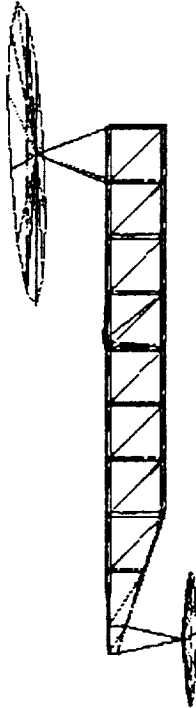
- [1] Vos, R.G.; Beste, D.L.; and Gregg, J., "Integrated Analysis Capability (IAC) User Manual (Level 2.5)", Boeing Aerospace & Electronics, Seattle, Washington, 1989.
- [2] Messac, A., "Optimal Simultaneous Structural and Control Design of Large Space Structures", Ph.D. thesis, Massachusetts Institute of Technology, Cambridge, Massachusetts, November 1985.
- [3] Khot, N.S.; Venkayya, V.B.; and Eastep, F.E., "Optimal Structural Modifications to Enhance the Active Vibration Control of Flexible Structures", *AIAA Journal*, Vol. 24, August 1986, pp. 1368-74.
- [4] Miller, D.F. and Shim, J., "Gradient Based Combined Structural and Control Optimization", *Journal of Guidance, Control, and Dynamics*, Vol. 10, May-June 1987, pp. 291-8.
- [5] Onoda, J. and Haftka, R.T., "An Approach to Structure/Control Simultaneous Optimization for Large Flexible Spacecraft", *AIAA Journal*, Vol. 25, August 1987, pp. 1133-8.
- [6] Morrison, S.K.; Ye, Y.; Gregory, C.F., Jr.; Kosut, R.L.; and Regelbrugge, M.E., "Integrated Structural/Controller Optimization for Large Space Structures", *AIAA Guidance, Navigation, and Control Conference*, Minneapolis, Minnesota, 1988.
- [7] Milman, M.; Salama, M.; Scheid, R.; Bruno, R.; and Gibson, J., "Integrated Control-Structure Design: A Multiobjective Approach", *JPL D-6767*, Jet Propulsion Laboratory, California Institute of Technology, January, 1990.
- [8] *PATRAN Users' Guide*, PDA Engineering, Santa Ana, California, September 1986.
- [9] *MACSYMA Reference Manual*, Document No. SMI0500030.013, Symbolics, Inc., Burlington, Massachusetts, November 1988.



- [10] Dailey, R.L., "Eigenvector Derivatives with Repeated Eigenvalues", *AIAA Journal*, Vol. 27, No. 4, April 1989, pp. 486-91.
- [11] Youla, D.C.; Jabr, H.A.; and Bongiorno, J.J., "Modern Wiener-Hopf Design of Optimal Controllers — Part II: The Multivariable Case," *IEEE Transactions on Automatic Control*, Vol. 21, pp. 319-38, June 1976.
- [12] Boyd, S.P.; Balakrishnan, V.; Barratt, C.H.; Khraishi, N.M.; Li, X.M.; Meyer, D.G.; and Norman, S.A., "A New CAD Method and Associated Architectures for Linear Controllers," *Technical Report No. L-104-86-1*, Stanford University, December 1986.
- [13] Belvin, K., "EPS Structure Description", NASA Langley Research Center, June 1, 1989.
- [14] Gregory, C.Z., "Reduction of Large Flexible Spacecraft Models Using Internal Balancing Theory", *AIAA Guidance and Control Conference*, Gatlinberg, Tennessee, August 1983.
- [15] Skelton, R.E., *Dynamic Systems Control: Linear Systems Analysis and Synthesis*, John Wiley and Sons, 1988.
- [16] Francis, B.A. and Doyle, J.C., "Linear Control Theory with an  $H_\infty$  Optimality Criterion", *SIAM J. Cont. Optim.*, Vol. 25, No. 4, July 1987, pp. 815-44.

## **Appendix A**

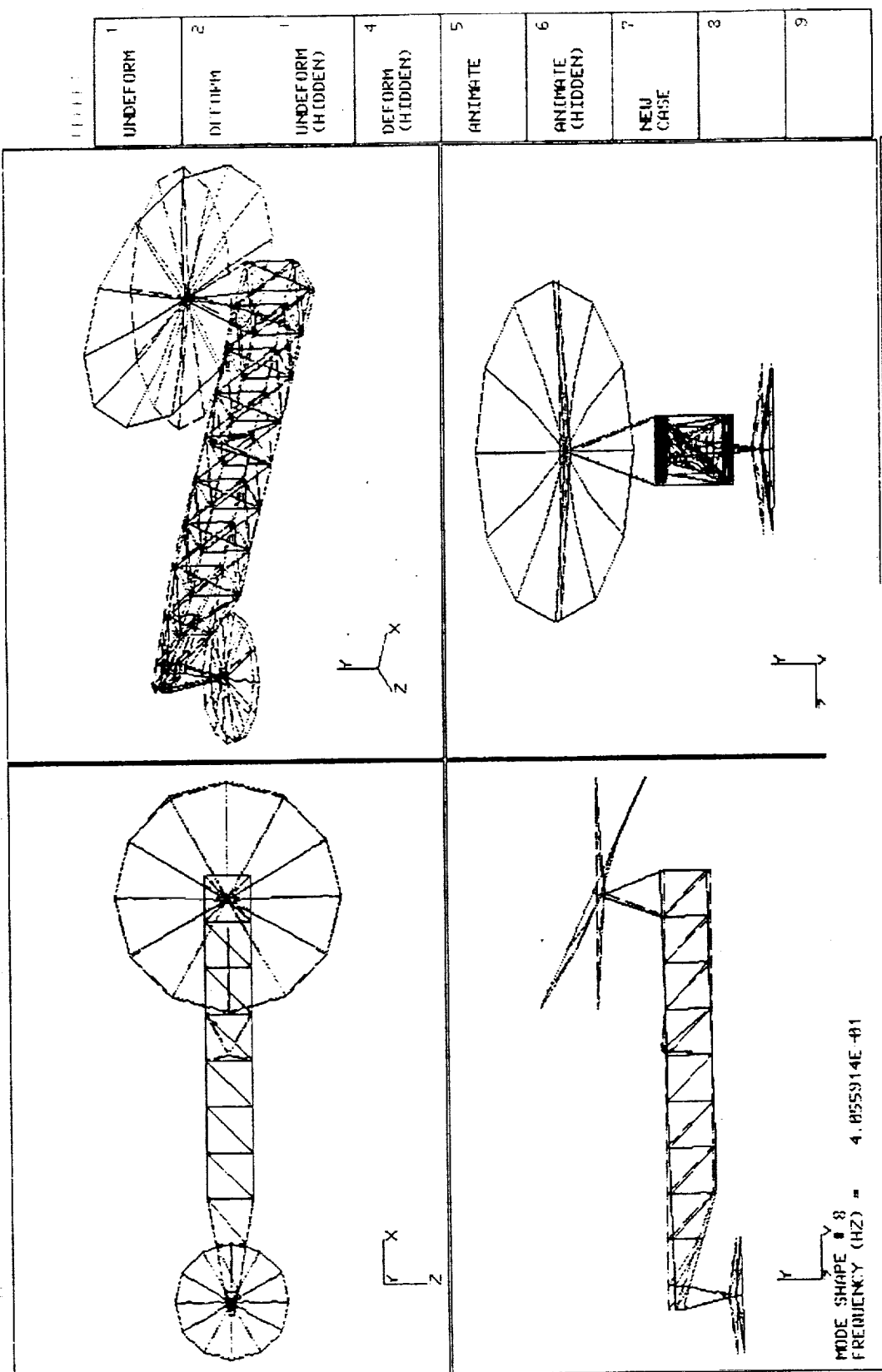
This appendix contains plots showing the mode shapes of the first 16 flexible modes of the baseline EPS structure. These are screen copies from an interactive PATRAN session.

1	UNDEFORM		
2	DEFURM		
3	UNDEFORM (HIDDEN)		
4	DEFORM (HIDDEN)		
5	ANIMATE		
6	ANIMATE (HIDDEN)		
7	NEW CASE		
8			
9			

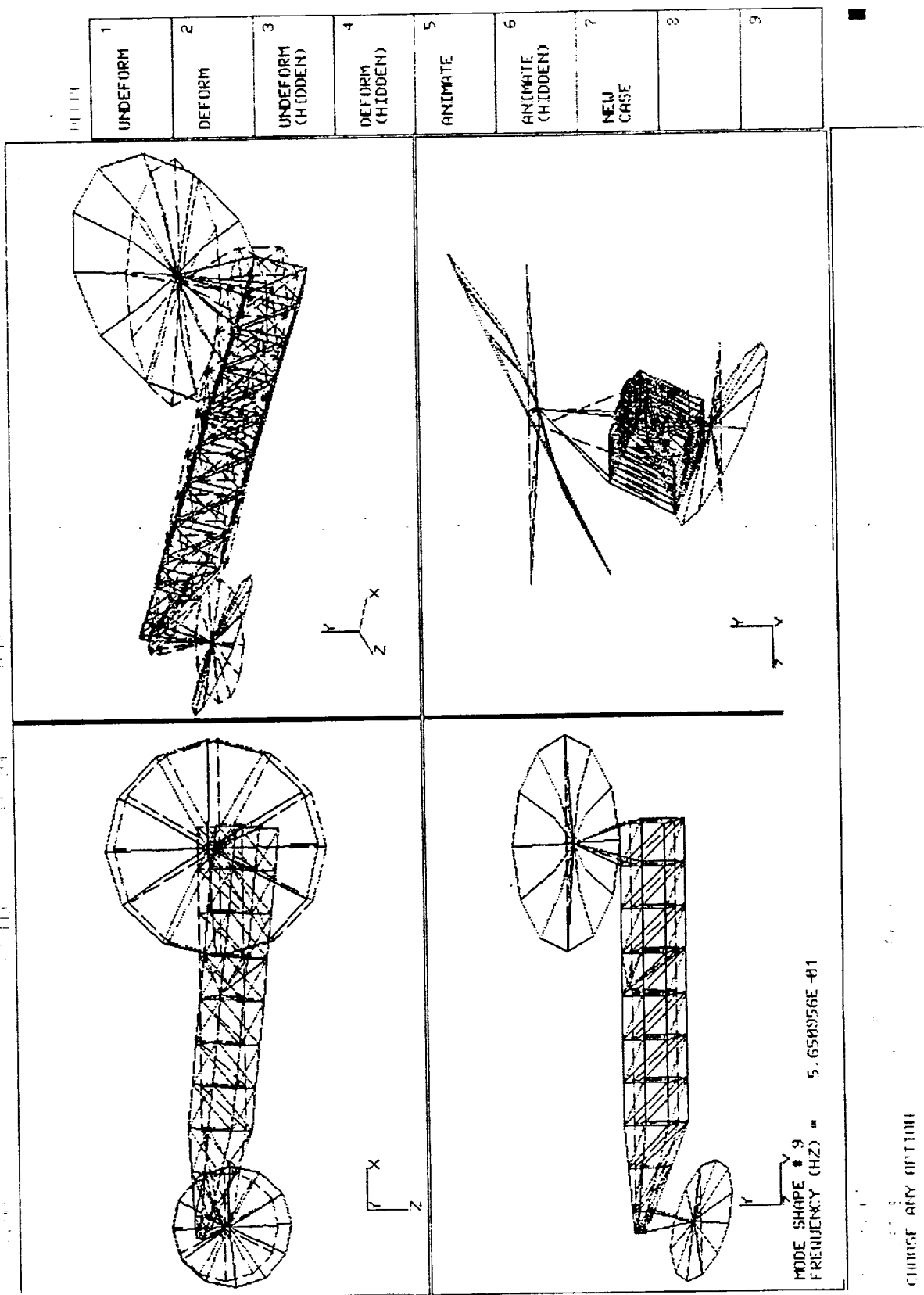
MIDE SHAPE 7

FREQUENCY (HZ) = 2.422458E+01

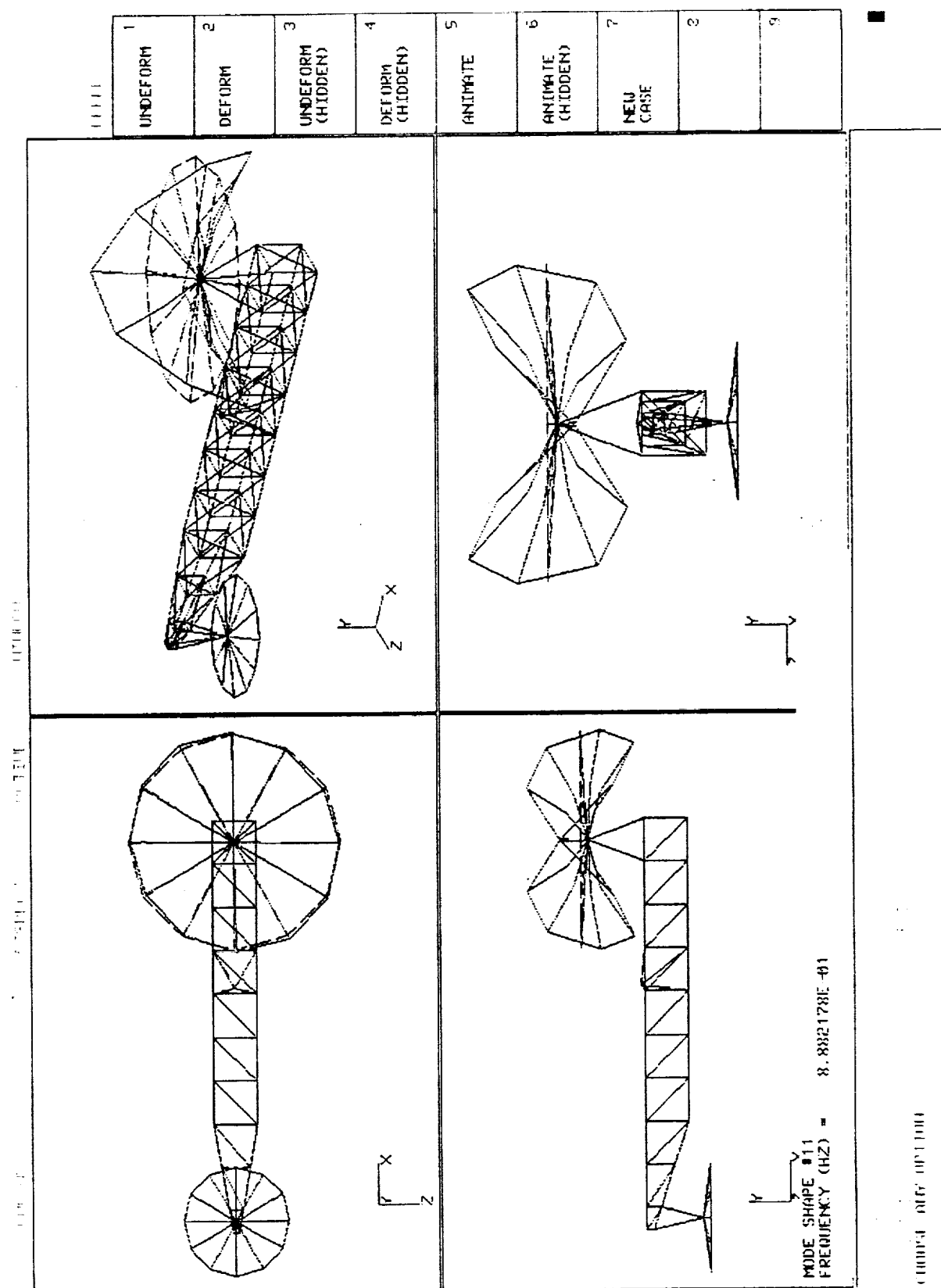
CHOOSE ANY OPTION

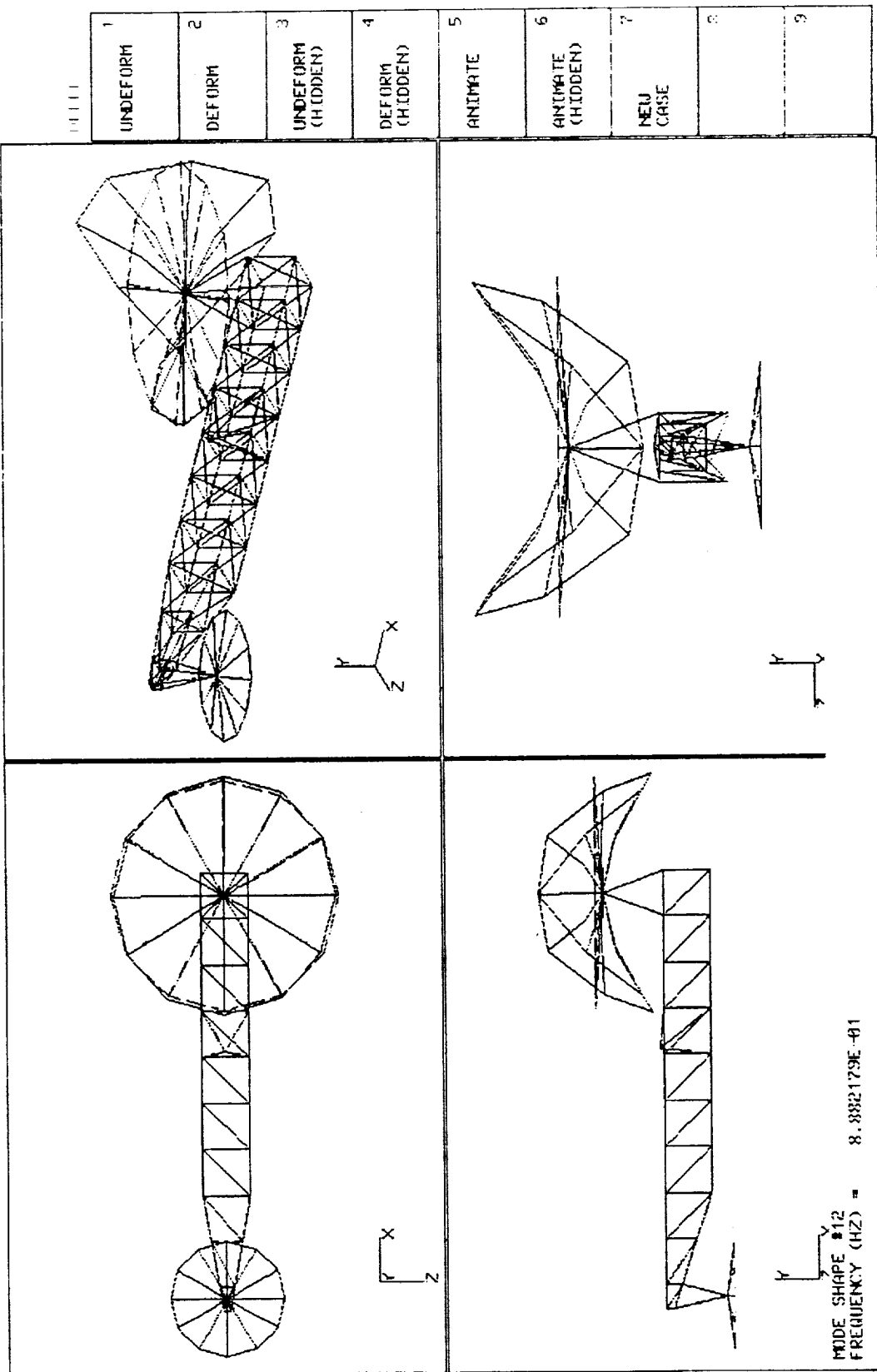


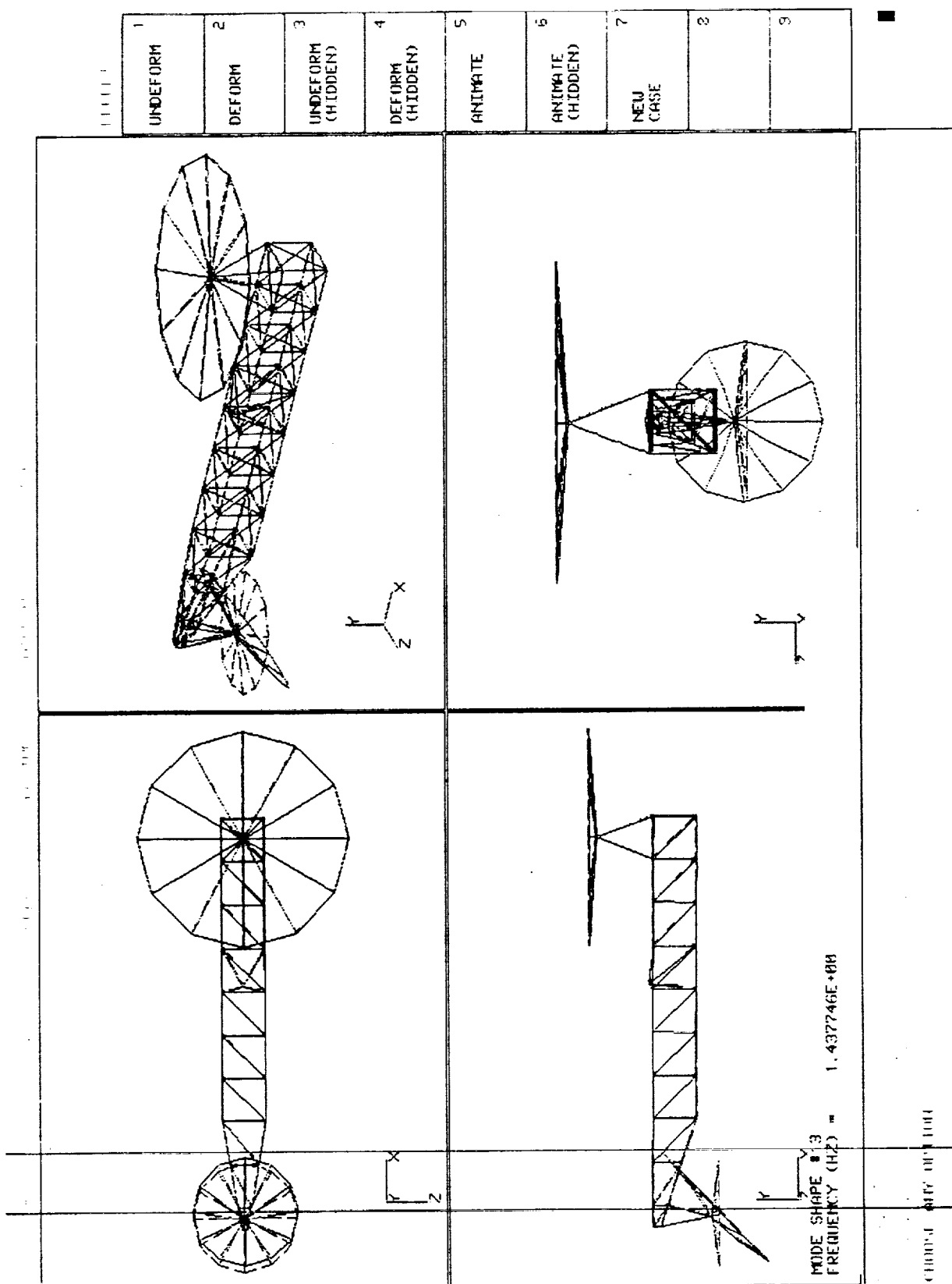
MODE SHAPE 8.8  
FREQUENCY (HZ) = 4.855914E-01



1	UNDEFORM
2	DEFORM
3	UNDEFORM (HIDDEN)
4	DEFORM (HIDDEN)
5	ANIMATE
6	ANIMATE (HIDDEN)
7	NEW CASE
8	
9	

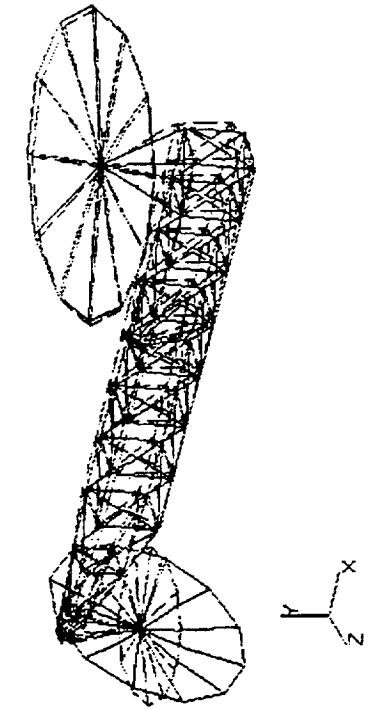
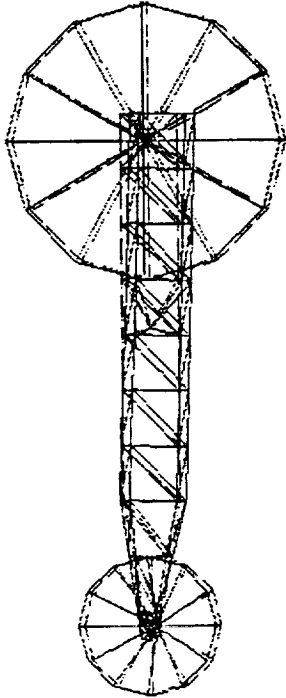
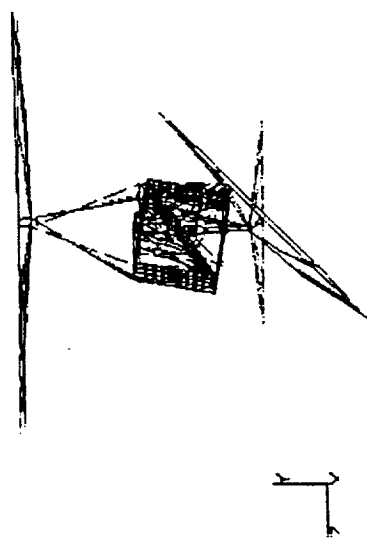
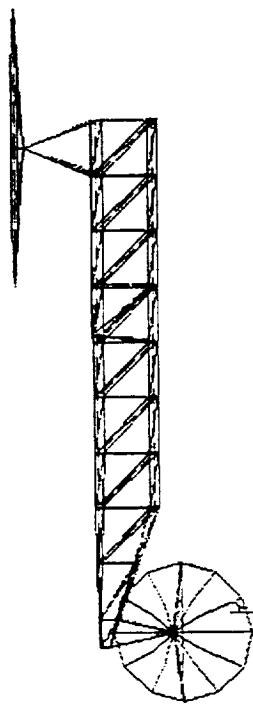






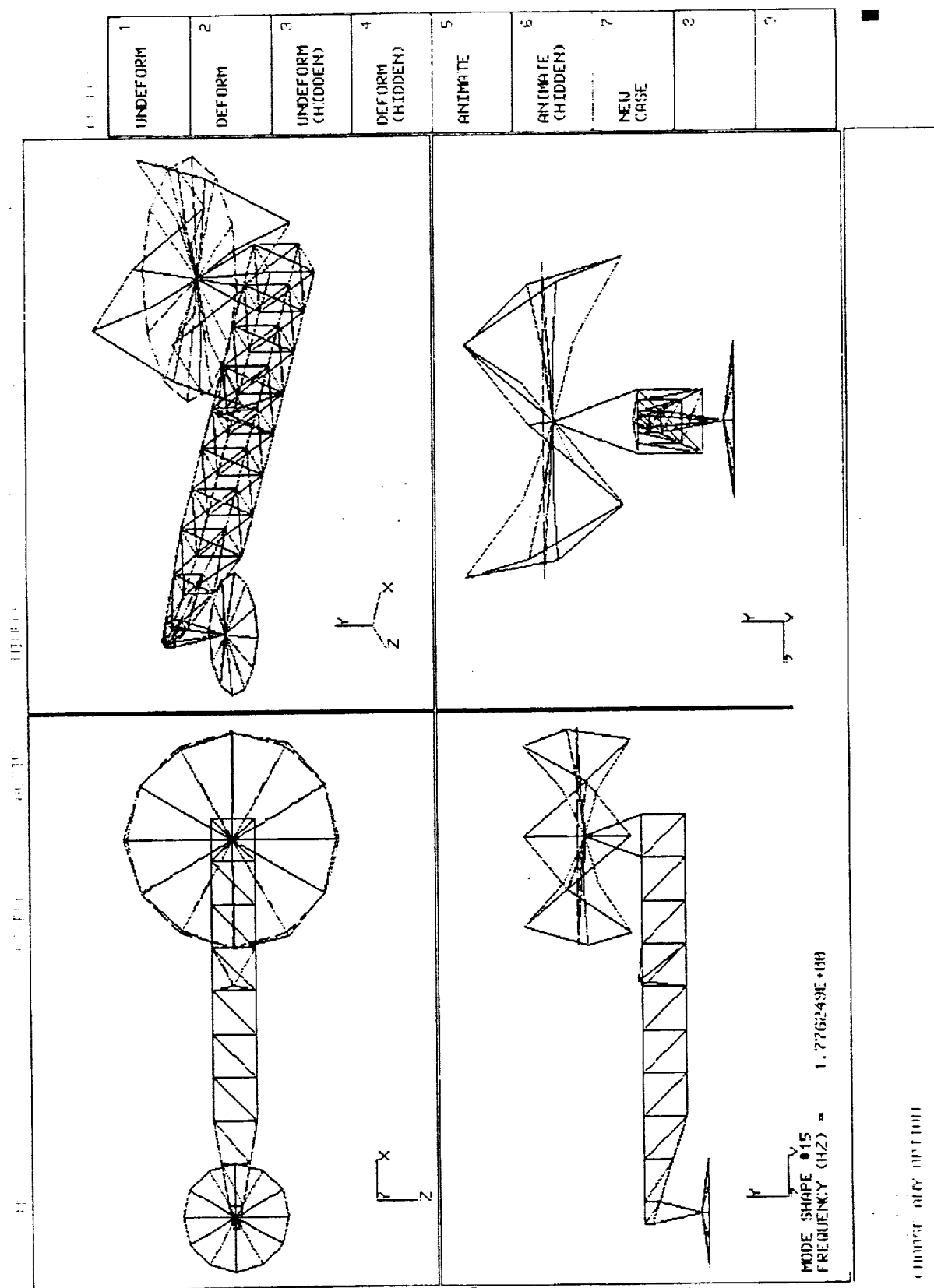
1	UNDEFORM
2	DEFORM
3	UNDEFORM (HIDDEN)
4	DEFORM (HIDDEN)
5	ANIMATE
6	ANIMATE (HIDDEN)
7	NEW CASE
8	
9	

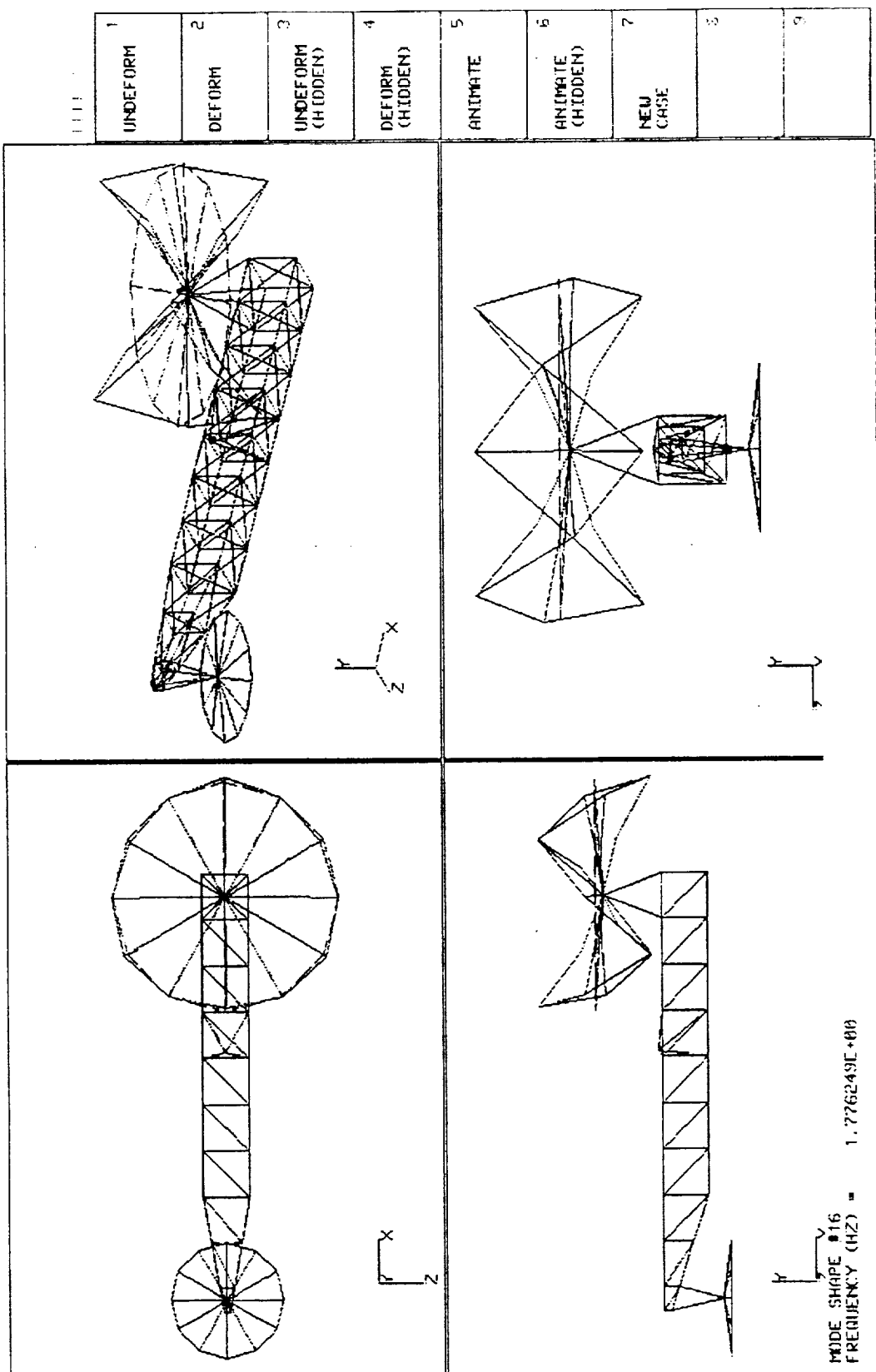


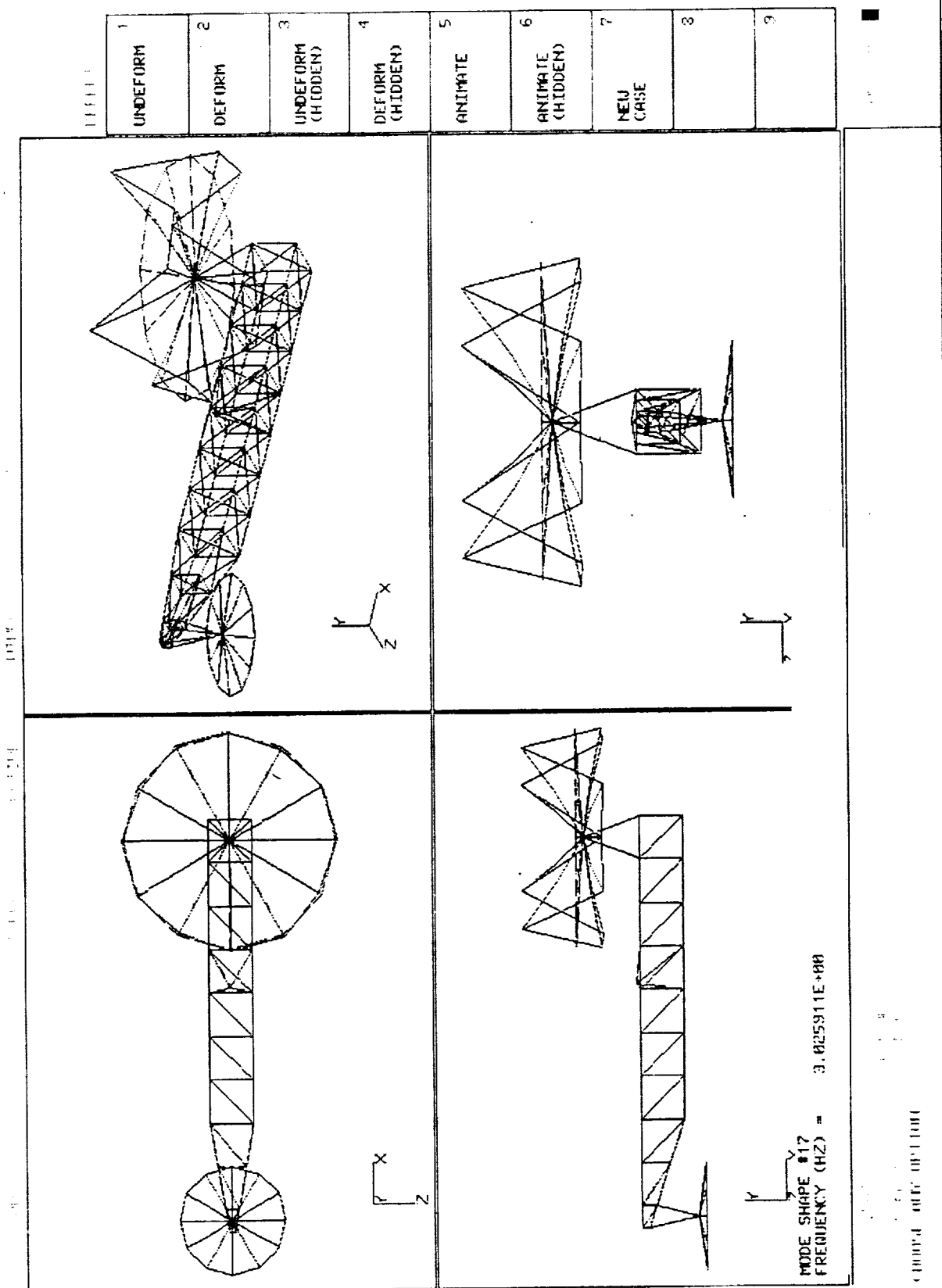
1	UNDEFORM		
2	DEFORM		
3	UNDEFORM (HIDDEN)		
4	DEFORM (HIDDEN)		
5	ANIMATE		
6	ANIMATE (HIDDEN)		
7	NEW CASE		
8			
9			

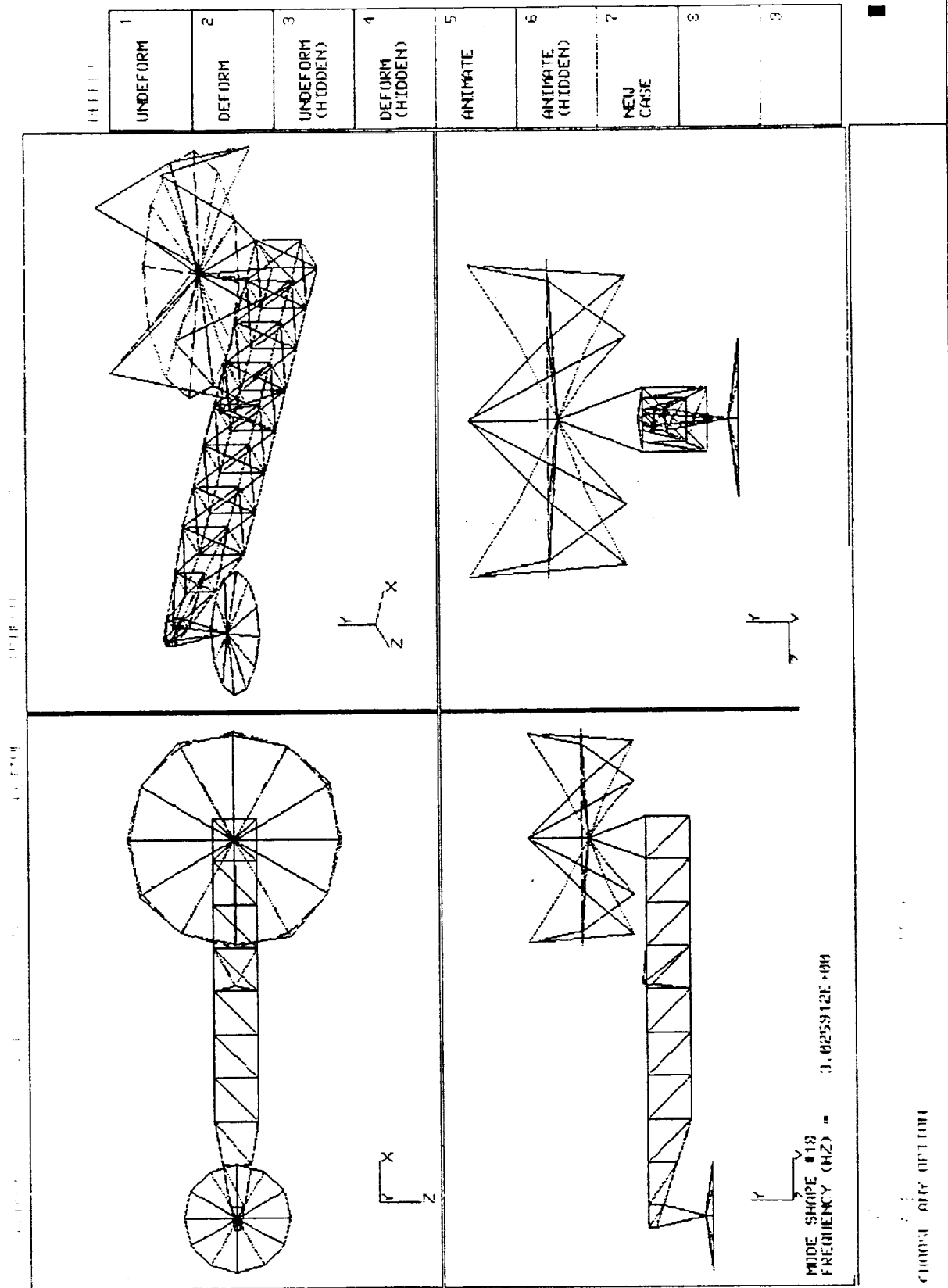
MIDC SHAPE #14  
 FREQUENCY (HZ) = 1.535942E+00

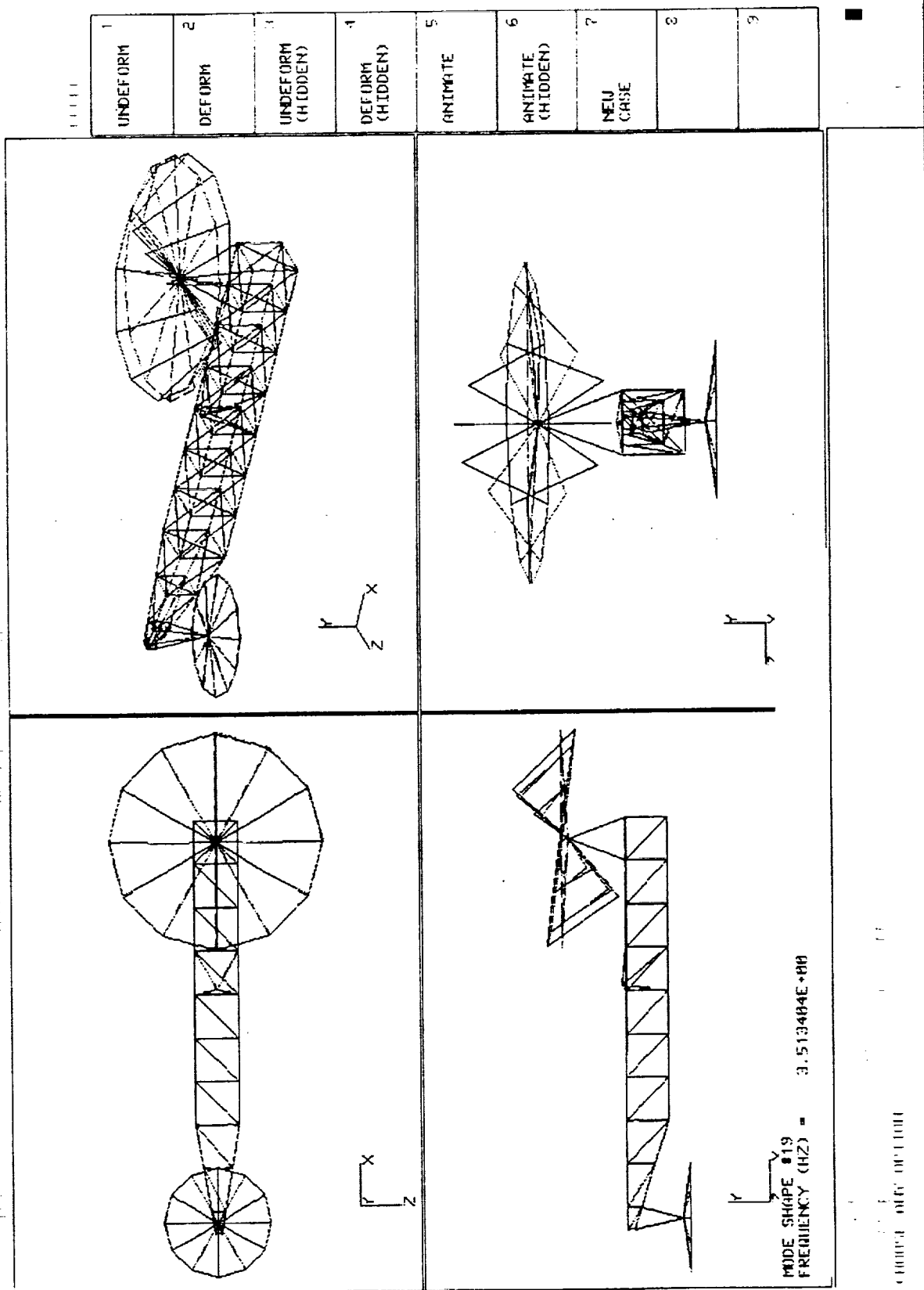
CHOOSE ANY OPTION

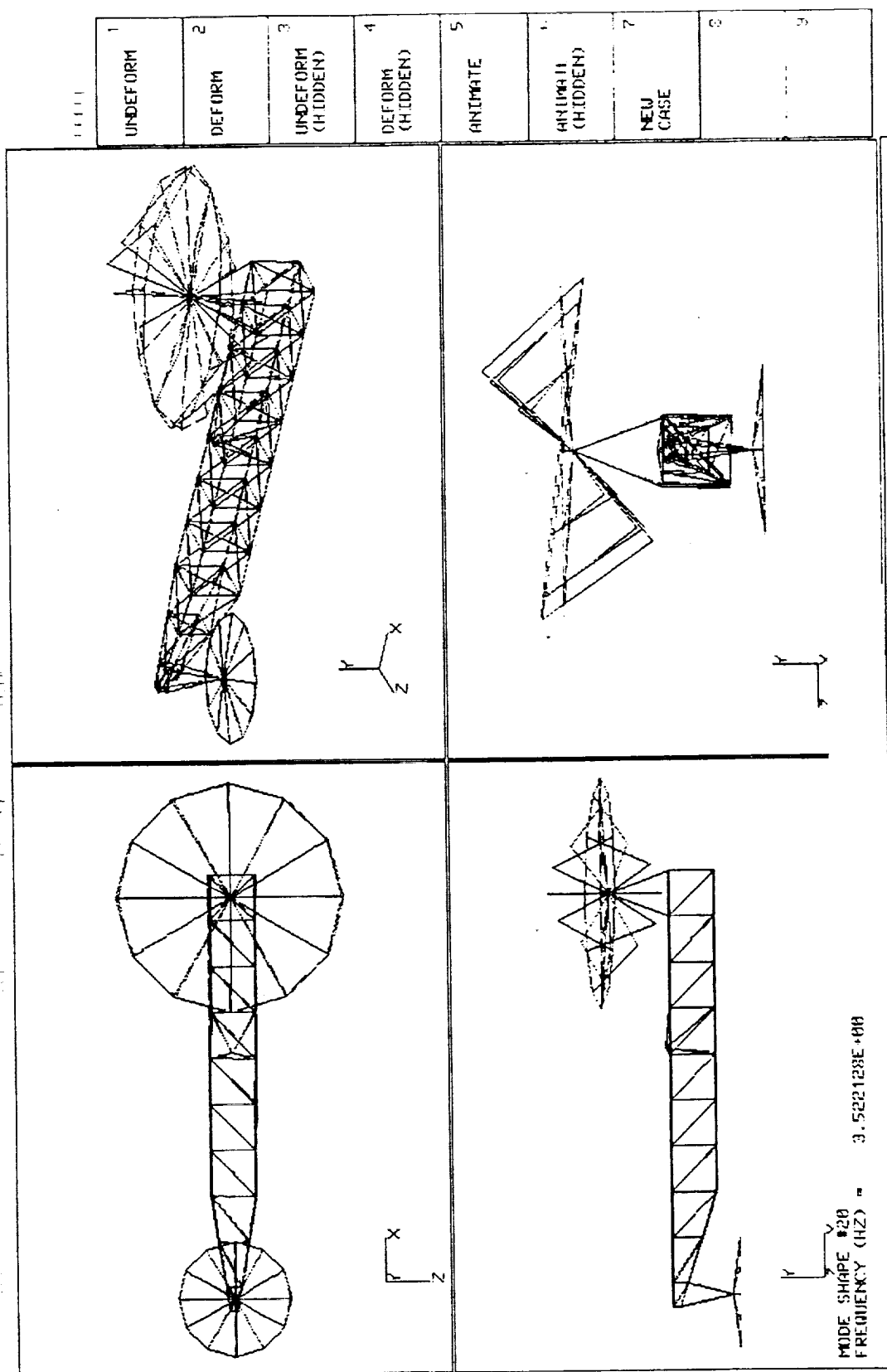


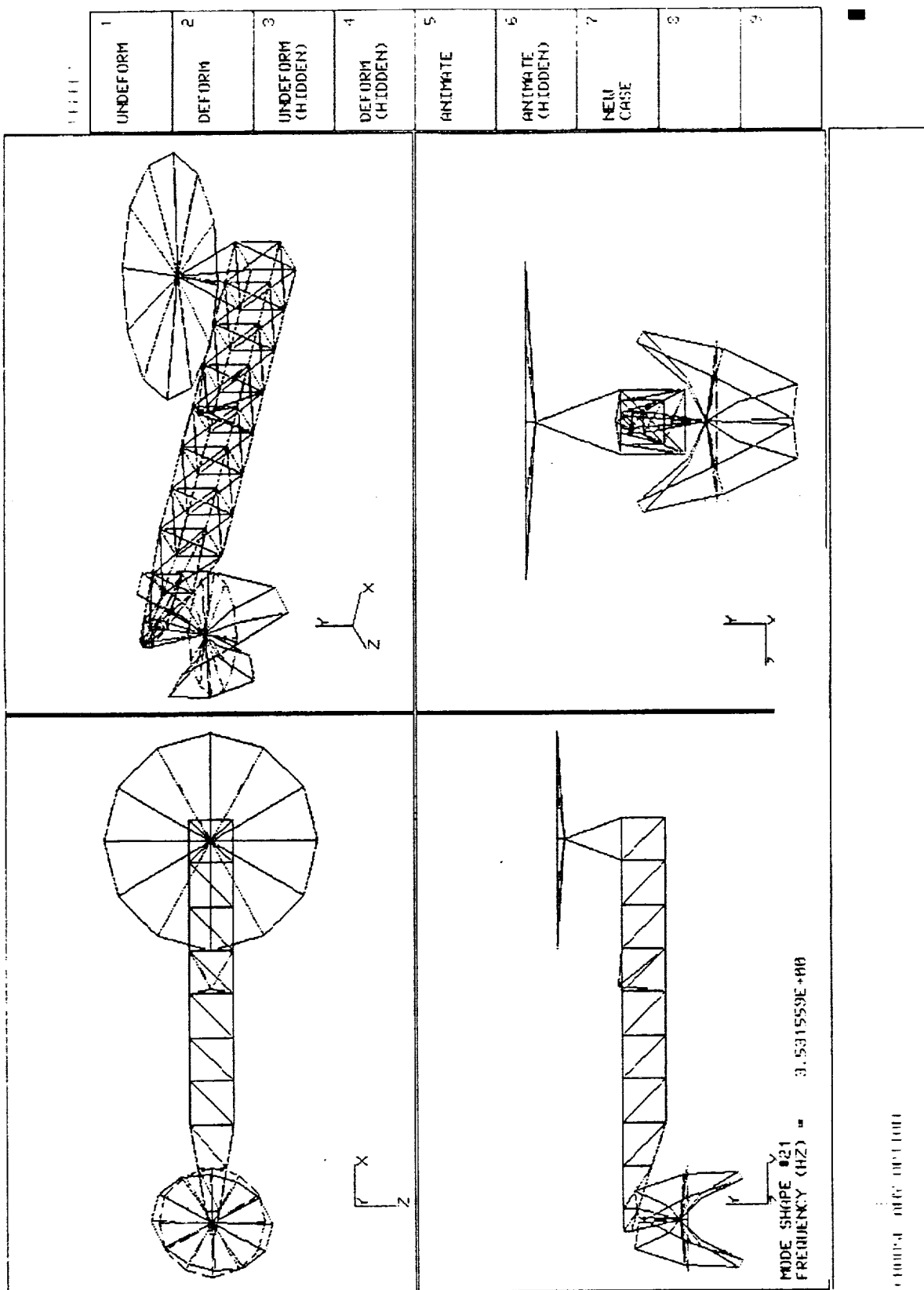




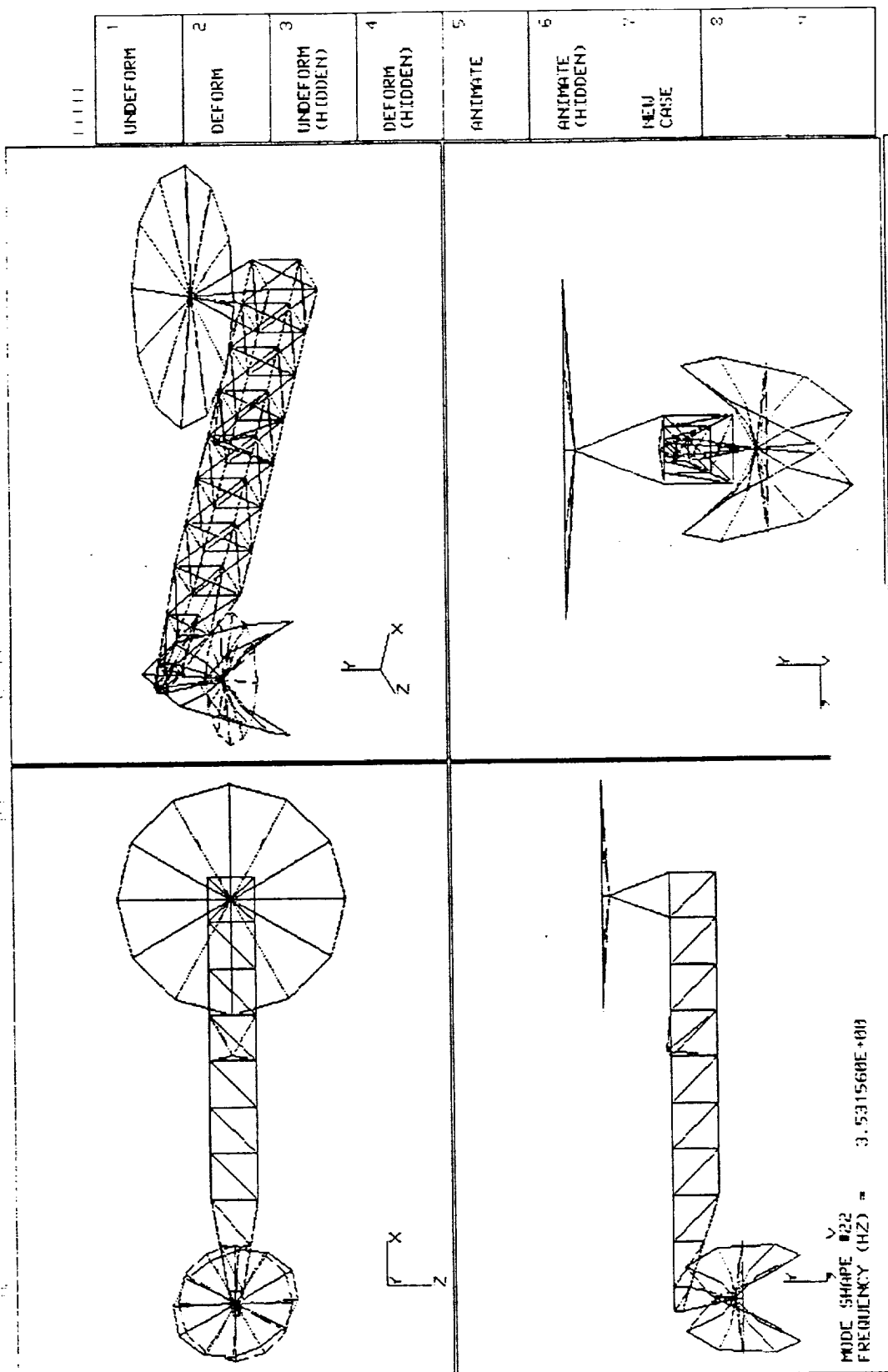












## Appendix B

# On $Q$ -Design

*Prepared by:*

Dr. Robert L. Kosut

Dr. Güntekin M. Kabuli

**Integrated Systems Inc.**

2500 Mission College Boulevard  
Santa Clara, California 95054-1215

# 1 Introduction

Consider a linear time-invariant finite-dimensional discrete-time plant described by the transfer function  $P$  (see Figure 1);  $w$ ,  $z$ ,  $u$  and  $y$  denote the exogenous inputs, regulated outputs, actuator inputs and sensor outputs, respectively. Typically,  $P$  represents the augmented plant; the original plant  $P_{yu}$  (the block of  $P$  representing the transfer function from  $u$  to  $y$ ) is augmented with stable blocks used as weights when taking into account the exogenous inputs and regulated outputs. In general, all that is required is that the unstable poles of  $P$  are in  $P_{yu}$ . With this assumption (which is in fact a necessary and sufficient condition for internal stabilization of the closed-loop system in Figure 1 by dynamic compensation) the set of all compensators  $C$  that stabilize  $P$  in Figure 1 is the set of all compensators that stabilize  $P_{yu}$ .

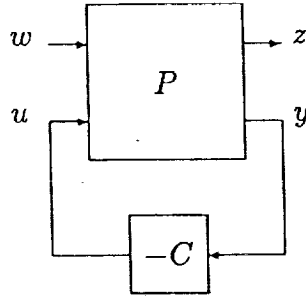


Figure 1: Closed-loop system

For a given lightly-damped flexible space structure with position and/or rate measurements, the transfer function  $P_{yu}$  is stable (poles in the open unit disk) and strictly-proper ( $P_{yu}(\infty) = 0$ ). Hence, the set of all proper compensators  $C$  such that the closed-loop system in Figure 1 is stable is given by

$$\{ Q(I - P_{yu}Q)^{-1} \mid Q \text{ is proper and stable} \} . \quad (1)$$

Using the parametrization in (1), the set of all achievable stable closed-loop transfer functions  $H_{zw}$  is given by

$$\{ P_{zw} - P_{zu}QP_{yw} \mid Q \text{ is proper and stable} \} . \quad (2)$$

## 2 Problem Description

Once the complete solution to all achievable closed-loop transfer functions is parametrized, one can conceivably improve (if possible) the closed-loop performance by reducing an objective function of  $H_{zw}$  over the parameter  $Q$  (from now on referred to as the  $Q$ -design). However the set of all realizable stable transfer functions can not be parametrized by a finite number of real parameters. Nevertheless, by increasing the number of real parameters, a sequence of parameter optimizations can be performed until the desired improvement in performance is achieved (as in QDES). Note that for an  $n_i$  input  $n_o$  output plant  $P_{yu}$ , an  $N$ th order FIR approximation requires  $N \cdot n_i \cdot n_o$  parameters.

The problem is to find a “suitable” class of stable transfer functions  $\{Q_q\}_{q \in \mathbb{R}^N}$  for the specific plant at hand such that  $N$  is “small” and minimization over  $q \in \mathbb{R}^N$  achieves the desired performance improvement.

Provided that a “suitable” parametrization of stable  $Q$  is available, the strong points of  $Q$ -design can be summarized as follows:

- As long as the design problem is approximated as a parameter optimization problem, the objective function can include both time- and frequency-domain constraints (choosing the objective function convex in the parameters definitely helps). Such a mix is not suitable in the conventional  $\mathcal{H}_2$ - and  $\mathcal{H}_\infty$ -design methods.
- If the input-output description is already given by impulse responses, there is no need for a model identification until the compensator is to be implemented. Since the feedback stabilization problem is already taken care of, each objective function evaluation need not be done after a stabilizing feedback law is calculated using conventional design methods, relying on the identified model.
- All three of the transfer functions in (2) (namely,  $P_{zw}$ ,  $P_{zu}$  and  $P_{yw}$ ) depend on the open-loop plant (the weights introduced during augmenting  $P_{yu}$  are stable cascaded blocks which do not introduce any feedback paths). Hence if the plant is also to be parameter optimized, the plant parameters are simply appended to those of  $Q$ .

In the rest of this report, we focus on a case study and a simplified SISO model of the EPS (Earth Pointing Satellite). As a benchmark comparison,  $Q$ -design is compared against  $\mathcal{H}_2$ -design.

### 3 Method used for SISO $P_{yu}$

Suppose that there is one actuator and one sensor. Let the transfer matrices  $T_1$  and  $T_2$  be defined as follows:

$$\begin{aligned} T_1 &:= P_{zw} \\ T_2 &:= P_{zu}P_{yw} . \end{aligned}$$

The following steps are taken to compute the optimal (in the  $\mathcal{H}_2$ -norm sense, over a parametrization  $Q_q : q \in \mathbb{R}^N$ ) norm of the transfer matrix

$$H_{zw} = T_1 - Q_q T_2 :$$

1. Determine the number of samples  $N_{\text{samples}}$ ; get the impulse response sequences for the transfer matrices  $T_1$  and  $T_2$ .
2. Choose a numerator polynomial  $n$  and a strictly-Hurwitz denominator polynomial  $d$  of the same order. Determine the number of taps  $N_{\text{taps}}$ . Set

$$Q_q = \frac{n}{d} \sum_{i=1}^{N_{\text{taps}}} q_i z^{-i} ;$$

we choose the FIR term strictly-proper since the optimal  $Q$  for a proper plant is strictly-proper.

3. Filter the pulse sequences of  $T_2$  with  $\frac{n}{d}$ :

$$T_2 \leftarrow T_2 \frac{n}{d} .$$

4. Determine a solution  $q$  of

$$\text{argmin} \left\| T_1 - T_2 \sum_{i=1}^{N_{\text{taps}}} q_i z^{-i} \right\|_2$$

from the minimum norm least squares solution of

$$y = A \begin{bmatrix} q_1 \\ \vdots \\ q_{N_{\text{taps}}} \end{bmatrix} ,$$

where  $y$  and  $A$  can be obtained by reordering the entries of  $T_1$  and  $T_2$ . To find the solution, there is no need construct  $y$  and  $A$  completely; in our cases  $w, z \in \mathbb{R}^2$  and  $N_{\text{samples}} = 5000$  and  $10000$ . Instead, form  $A^T A \in \mathbb{R}^{N_{\text{taps}} \times N_{\text{taps}}}$  and  $A^T y \in \mathbb{R}^{N_{\text{taps}}}$ . Get the minimum norm least-squares solution

$$\hat{q} = (A^T A) \setminus (A^T y) .$$

Compute the least-squares error  $\|y - A\hat{q}\|_2$  without constructing  $A$ .

5. Plug the compensator

$$C = Q_{\hat{q}}(1 - P_{yu}Q_{\hat{q}})^{-1}$$

in the feedback loop.

6. Compute the  $\mathcal{H}_2$ -norm analytically from the state-space description of the closed-loop map  $H_{zw}$  and check against step 4 .

## 4 Case Study

Let  $G$  denote the zero-order hold equivalent (sampled at  $50 \text{ Hz}^{-1}$ ) of the transfer function  $\frac{1}{s^2+0.1s+1}$ . Let  $P$  in Figure 1 be given by

$$\begin{bmatrix} z_1 \\ z_2 \\ y \end{bmatrix} = \begin{bmatrix} 100G & 0 & 100G \\ 0 & 0 & 0.1 \\ G & 0.01 & G \end{bmatrix} \begin{bmatrix} w_1 \\ w_2 \\ u \end{bmatrix}. \quad (3)$$

Discrete-time  $\mathcal{H}_2$ -optimal design gives  $\|H_{zw}\|_{2,\text{opt}} = 0.8225$ .

We chose  $N_{\text{samples}} = 5000$  (5 time constants). Let

$$n = d = 1.$$

For a given  $N_{\text{taps}}$ , let

$$Q_q = \sum_{i=1}^{N_{\text{taps}}} q_i z^{-i}.$$

For different number of taps,  $\|H_{zw}\|_{2,\text{EXE}}$  (the computed least-squares error  $\|y - Aq\|_2$  using the executables) and  $\|H_{zw}\|_{2,\text{SYS}}$  ( $\mathcal{H}_2$ -norm from the system matrix description of the closed-loop map  $H_{zw}$  obtained by plugging in the compensator  $Q_q(1 - P_{yu}Q_q)^{-1}$ ) are listed in Table 1.

$N_{\text{taps}}$	$\ H_{zw}\ _{2,\text{EXE}}$	$\ H_{zw}\ _{2,\text{SYS}}$
1	31.5830	31.5839
5	2.1230	2.1241
10	1.6210	1.6215
20	0.8513	0.8514

Table 1: Optimal FIR approximations for different number of taps; optimal  $\mathcal{H}_2$ -norm is 0.8225.

Note that column 2 in Table 1 is computed from the 5000 samples of the impulse responses of  $P_{zw}$ ,  $P_{zu}$  and  $P_{yw}$ . Column 3 is obtained from the closed-loop system in Figure 1, where the plant  $P$  is represented by the state-space description. The close results are due to considerably high sampling rate and long pulse sequence used in the computations. For a larger scale problem, one should be cautious in assigning the sampling rate and sample size, trading off computational burden versus aliasing.

<sup>1</sup>Continuous-time  $\mathcal{H}_2$ -optimal design for the plant description where  $G$  in (3) is replaced by  $\frac{1}{s^2+0.1s+1}$  results in a compensator eigenvalue magnitude of 41.56 rad/s. The sampling rate was chosen approximately 7.5 times faster to get the discrete-time optimal design performance similar to the continuous-time frequency plots.

In order to reduce the number of parameters (  $N_{\text{taps}}$  ), an initial check was made by assigning

$$\begin{aligned} n &= z^4 \\ d &= \prod_{i=1}^4 (z - p_i) \\ Q_q &= \frac{n}{d} \sum_{i=1}^4 q_i z^{-i} , \end{aligned}$$

where the preassigned  $p_i$  's denote the optimal  $Q$  pole locations. Solving for this 4 parameter  $Q$  representation (  $Q_q$  ), we obtained

$$\begin{aligned} \|H_{zw}\|_{2,\text{EXE}} &= 0.8306 \\ \|H_{zw}\|_{2,\text{SYS}} &= 0.8306 . \end{aligned}$$

Clearly, this 4 parameter representation of  $Q$  achieves a better result than the 20 parameter FIR representation in Table 1 . However, one does not have access to the optimal pole locations to start with.

A couple of other  $d$  assignments were done as follows: for a fixed radius  $r$  , the four poles were spread as  $re^{\pm j\theta_k}$  where  $\theta_k \in [0, \theta_{\max}]$  . For  $[\theta_1 \ \theta_2] = [0.1 \ 0.5]$  , we obtained  $\|H_{zw}\|_{2,\text{EXE}} = \|H_{zw}\|_{2,\text{SYS}} = 1.0645, 0.8969$  for  $r = 0.95$  and  $0.8$ , respectively. Both of these trials did better than a straightforward 4th order FIR approximation (2.89) .

The motivation is to preassign a structure for  $Q$  as in Section 3 (typically a stable factor of the inverse of the plant) and fine tune with the FIR factor, hopefully over a smaller number of parameters. If the openloop plant is to be designed taking into account the performance objective desired from a feedback law, this preassigned structure will be at most in the order of the plant and depend only on the plant parameters. Note that an identification approach in assigning the numerator and denominator coefficients of  $Q$  may not be useful due to the constraint that the parameter  $Q$  is stable.



## 5 EPS Model

In order to try out the idea involving the plant inversion, an SISO approximation of the original 32-state EPS model is obtained. The procedure is explained below.

Consider the 32-state state space description of EPS:

$$\begin{aligned}
 \dot{x} &= Ax + B_{\text{thr}}d_{\text{thr}} + B_{\text{act}}u_{\text{act}} \\
 \begin{bmatrix} y_{\text{los1}} \\ y_{\text{los2}} \end{bmatrix} &= C_{\text{los}}x \\
 d_{\text{thr}} &:= f_{z45} \\
 u_{\text{act}} &:= [f_{\theta42} \ f_{\phi42} \ f_{\psi42}]^T \\
 y_{\text{los1}} &:= [\theta_{26} \ \psi_{26}]^T \\
 y_{\text{los2}} &:= [\theta_{71} \ \psi_{71}]^T .
 \end{aligned} \tag{4}$$

There are 16 modes ranging from 0.2423 Hz to 3.5317 Hz . The damping ratio is  $\zeta = 0.02$  .

The four singular-value plots of the openloop plant in (4) are shown in Figure 2 .

### 5.1 Simplified EPS Model

We used the following 3 mode reduced model in (5) for the EPS :

$$\begin{aligned}
 \dot{x} &= \bar{A}x + \bar{B}_{\text{thr}}d_{\text{thr}} + \bar{B}_{\text{act}}\bar{u} \\
 y_{\text{los}} &= \bar{C}_{\text{los}}x \\
 \bar{u} &:= f_{\theta42} \\
 y_{\text{los}} &:= \theta_{71}
 \end{aligned} \tag{5}$$

obtained by the following MATRIX<sub>X</sub> commands:

```

SORIG32=[A BTHR BACT;CLOS 0*EYE(4)];
[SBAL SIG T]=BALANCE(SORIG32([1:10 35],[1:10 34]),10);
[AA BB CC DD]=SPLIT(SBAL,10);
BTHR=T\SORIG32(1:10,33);
ABAR = AA(1:6,1:6);
BBARTH = BTHR(1:6) ;
BBARACT = BB(1:6);
CBARLOS = CC(:,1:6);

```

The discrete-time model used for the EPS model is the zero-order hold equivalent (sampled at 300 Hz) of the 6-state plant description in (5).

The magnitude plots for the discrete-time 6-state EPS model are shown in Figure 3.

Compared with plots C and D in Figure 2 , plots A and B in Figure 3 match the frequency responses up to approximately 6 rad/s .

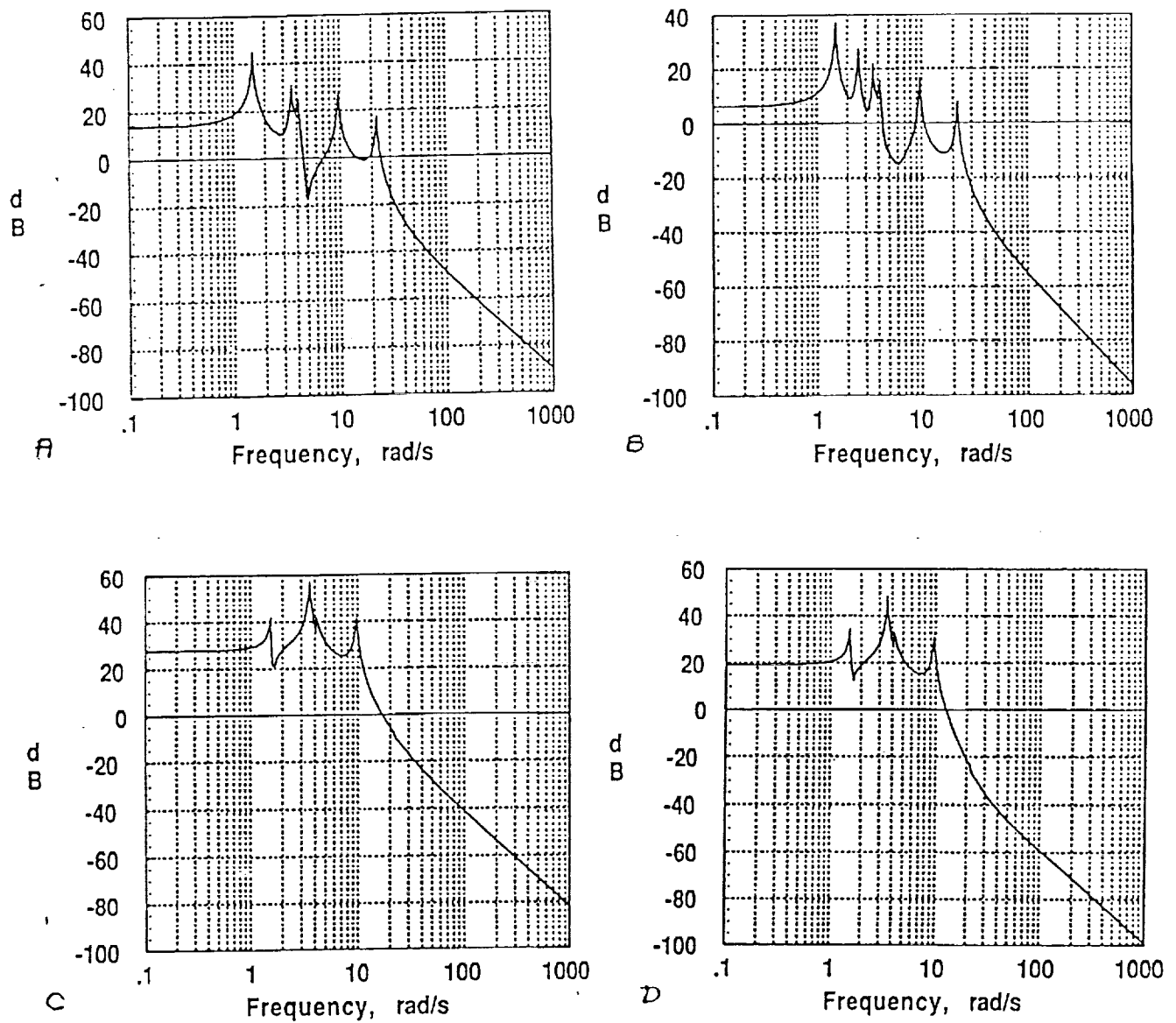


Figure 2:

The four singular-value plots of the plant in (4): A -  $d_{thr} \mapsto y_{los1}$ , B -  $u_{act} \mapsto y_{los1}$ ,  
C -  $d_{thr} \mapsto y_{los2}$ , D -  $u_{act} \mapsto y_{los2}$ .



## 6 Closed-loop Performance of SISO 6-State Discrete-Time EPS Model

Let  $G$  denote the zero-order hold equivalent (sampled at 300 Hz) of the 6-state plant description in (5) where

$$y_{\text{los}} = G_1 d_{\text{thr}} + G_2 \bar{u} .$$

Consider the augmented plant model

$$\begin{bmatrix} z_1 \\ z_2 \\ y \end{bmatrix} = \begin{bmatrix} 100G_1 & 0 & 100G_2 \\ 0 & 0 & 0.1 \\ G_1 & -0.01 & G_2 \end{bmatrix} \begin{bmatrix} w_1 \\ w_2 \\ u \end{bmatrix} . \quad (6)$$

Apply the feedback law

$$u = -Q_q(1 - G_2 Q_q)^{-1} y$$

as in Figure 1 , where  $Q_q$  is to be determined.

As a reference performance measure, discrete-time  $\mathcal{H}_2$ -optimal compensator is designed; the closed-loop yields  $\|H_{zw}\|_{2,\text{opt}} = 2.284$  . The magnitude plots for the four entries of the  $\mathcal{H}_2$ -optimal  $H_{zw}$  are shown in Figure 4. Comparing D in Figure 4 and B in Figure 3, the optimal  $Q$  magnitude plot is the negative of the  $P_{yu}$  plot (over the 0.3 rad range in Figure 3; taking into account the 60 dB shift due to the weights 0.1 and 0.01).

Sample size is chosen as  $N_{\text{samples}} = 10,000$  (approximately 1 time constant at 300 Hz). As in the case study in Section 4 , FIR approximations are made for different number of taps (  $Q_q = \sum_{i=1}^{N_{\text{taps}}} q_i z^{-i}$  ). Results are listed in Table 2:

$N_{\text{taps}}$	$\ H_{zw}\ _{2,\text{EXE}}$	$\ H_{zw}\ _{2,\text{SYS}}$
10	225.5873	277.0512
20	225.5419	276.6257
100	224.1206	269.1206

Table 2: Optimal FIR approximations for different number of taps; optimal  $\mathcal{H}_2$ -norm is 2.2840.

Note that, unlike Table 1,  $\|H_{zw}\|_{2,\text{EXE}}$  and  $\|H_{zw}\|_{2,\text{SYS}}$  (see section 4) are not close, due to 1 time constant truncation of the original pulse sequence. Despite large  $N_{\text{taps}}$  there is not a considerable improvement in the closed-loop  $\mathcal{H}_2$ - norm.

Instead, we chose

$$Q_q = \frac{n}{d} \sum_{i=1}^4 q_i z^{-i} , \quad (7)$$

where  $n$  has all six poles of  $G_2$  and  $d$  has all four stable zeros of  $G_2$  and two at zero (the two zeros at zero are chosen to make  $\frac{n}{d}$  relative degree zero; no specific reason for

assigning them at zero). Hence  $\frac{n}{d}$  represents the stable factor of the inverse of  $G_2$  and the four FIR parameters are introduced to fine tune. Calculations show that

$$\begin{aligned} \|H_{zw}\|_{2,\text{EXE}} &= 7.7974 \\ \|H_{zw}\|_{2,\text{SYS}} &= 3.2685 \text{ (optimal is 2.284)} \end{aligned}$$

The magnitude plots of the four entries of the final run  $H_{zw}$  with  $Q_q$  as in (7) are shown in Figure 5.

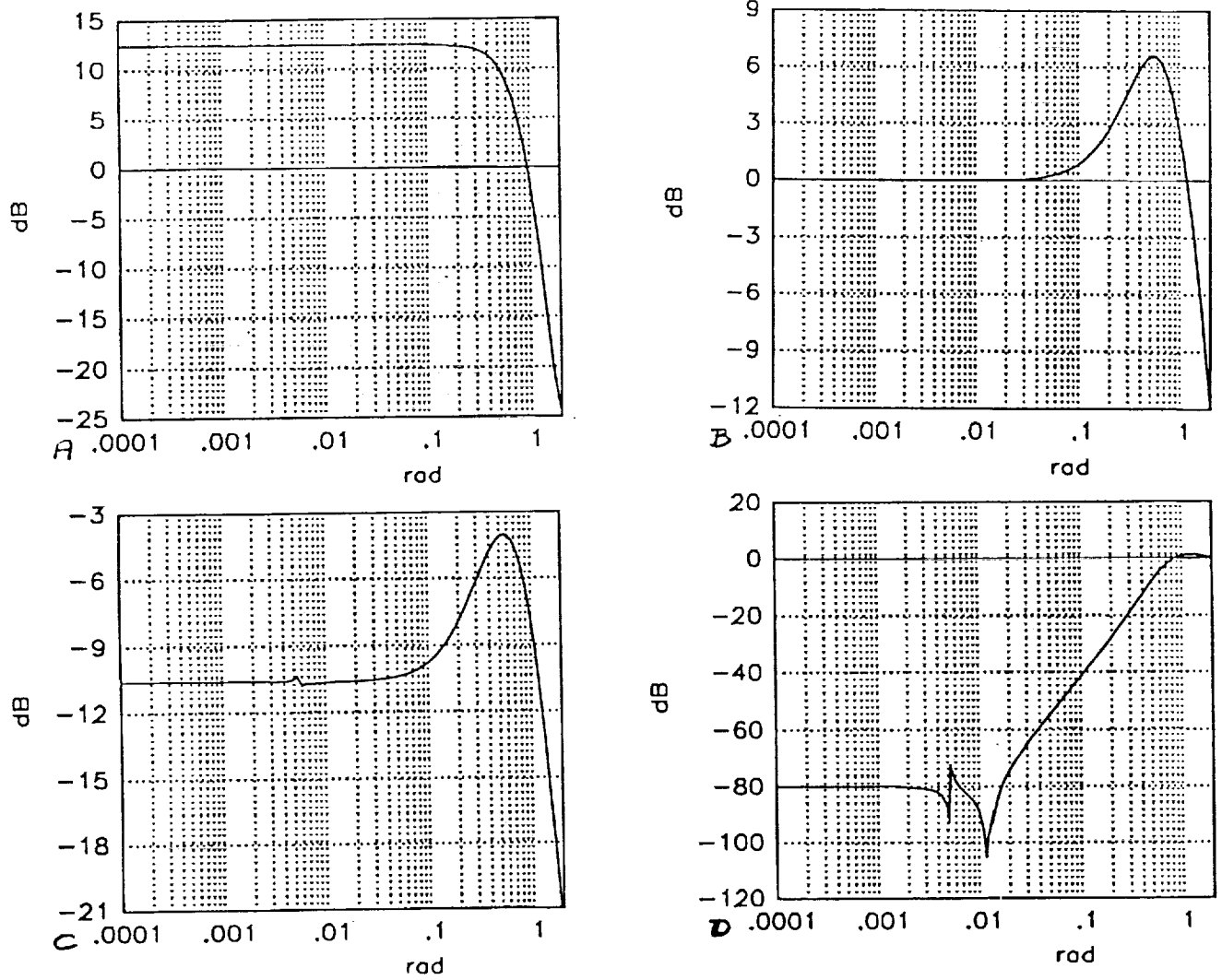


Figure 4:

The magnitude plots for the four entries of the  $\mathcal{H}_2$ -optimal  $H_{zw}$  for the plant description in (6): A -  $w_1 \mapsto z_1$ , B -  $w_2 \mapsto z_1$ , C -  $w_1 \mapsto z_2$ , D -  $w_2 \mapsto z_2$ .

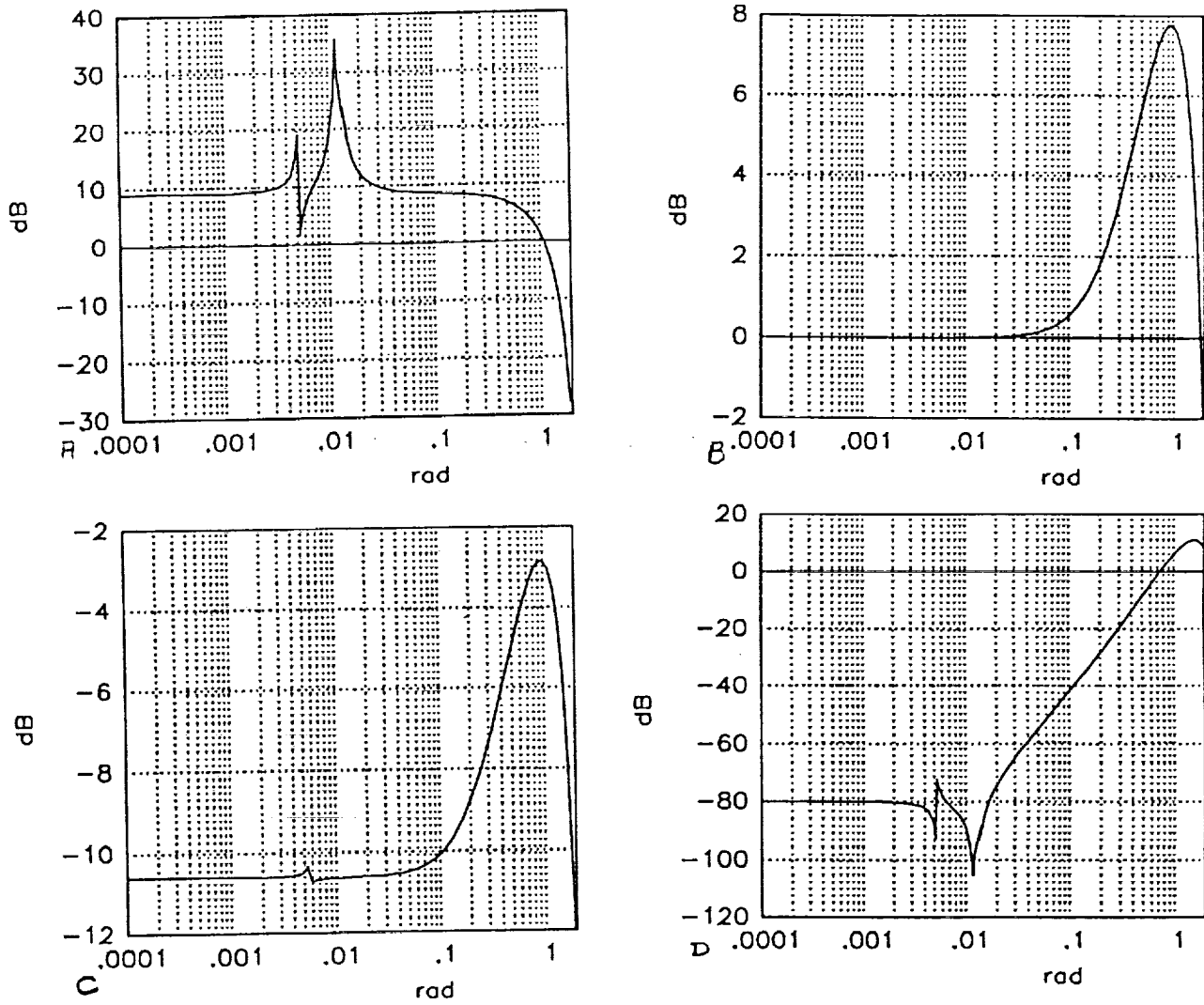


Figure 5:

The magnitude plots of the four entries of  $H_{zw}$  for the plant description in (6) and  $Q_q$  in (7): A -  $w_1 \mapsto z_1$  , B -  $w_2 \mapsto z_1$  , C -  $w_1 \mapsto z_2$  , D -  $w_2 \mapsto z_2$  .





## Report Documentation Page

1. Report No. NASA CR-182020		2. Government Accession No.		3. Recipient's Catalog No.	
4. Title and Subtitle Integrated Control-Structure Design				5. Report Date January 15, 1991	
				6. Performing Organization Code	
7. Author(s) K. Scott Hunziker and Raymond H. Kraft				8. Performing Organization Report No.	
9. Performing Organization Name and Address Boeing Aerospace P. O. Box 3999 Seattle, WA 92124-2499				10. Work Unit No. 506-14-51-01	
				11. Contract or Grant No. NAS1-18762	
12. Sponsoring Agency Name and Address National Aeronautics and Space Administration Langley Research Center Hampton, VA 23665-5225				13. Type of Report and Period Covered Contractor Report	
				14. Sponsoring Agency Code	
15. Supplementary Notes Langley Technical Monitor: Dr. Ernest S. Armstrong Task 3 Final Report					
16. Abstract <p>A new approach for the design and control of flexible space structures is described. The approach integrates the structure and controller design processes thereby providing extra opportunities for avoiding some of the disastrous effects of control-structures interaction and for discovering new, unexpected avenues of future structural design. A control formulation based on Boyd's implementation of Youla parametrization is employed. Control design parameters are coupled with structural design variables to produce a set of integrated-design variables which are selected through optimization-based methodology. A performance index reflecting spacecraft mission goals and constraints is formulated and optimized with respect to the integrated design variables. Initial studies have been concerned with achieving mission requirements with a lighter, more flexible space structure. Details of the formulation of the integrated-design approach are presented and results are given from a study involving the integrated redesign of a flexible geostationary platform.</p>					
17. Key Words (Suggested by Author(s)) Controls, Flexible Structures, Vibration Suppression, Optimization-based design, Integrated Design, Control-Structures Interaction, Youla parametrization, Nonlinear programming				18. Distribution Statement Unclassified--Unlimited Subject Category 18	
19. Security Classif. (of this report) Unclassified		20. Security Classif. (of this page) Unclassified		21. No. of pages 65	
				22. Price	

